

Alma Mater Studiorum Università di Bologna  
Archivio istituzionale della ricerca

Acynodon adriaticus from Villaggio del Pescatore (Campanian of Italy): Anatomical and chronostratigraphic integration improves phylogenetic resolution in Hylaeochampsidae (Eusuchia)

This is the final peer-reviewed author's accepted manuscript (postprint) of the following publication:

*Published Version:*

Marco M., Chiarenza A.A., Delfino M., Fabbri M., Milocco K., Fanti F. (2023). Acynodon adriaticus from Villaggio del Pescatore (Campanian of Italy): Anatomical and chronostratigraphic integration improves phylogenetic resolution in Hylaeochampsidae (Eusuchia). CRETACEOUS RESEARCH, 151, 1-21 [10.1016/j.cretres.2023.105631].

*Availability:*

This version is available at: <https://hdl.handle.net/11585/937301> since: 2024-05-20

*Published:*

DOI: <http://doi.org/10.1016/j.cretres.2023.105631>

*Terms of use:*

Some rights reserved. The terms and conditions for the reuse of this version of the manuscript are specified in the publishing policy. For all terms of use and more information see the publisher's website.

This item was downloaded from IRIS Università di Bologna (<https://cris.unibo.it/>).  
When citing, please refer to the published version.

(Article begins on next page)

This is the final peer-reviewed accepted manuscript of:

Marco M.; Chiarenza A.A.; Delfino M.; Fabbri M.; Milocco K.; Fanti F.: *Acynodon adriaticus* from Villaggio del Pescatore (Campanian of Italy): Anatomical and chronostratigraphic integration improves phylogenetic resolution in Hylaeochampsidae (Eusuchia)

CRETACEOUS RESEARCH VOL. 151 ISSN 0195-6671

DOI: 10.1016/j.cretres.2023.105631

The final published version is available online at:

<https://dx.doi.org/10.1016/j.cretres.2023.105631>

Terms of use:

Some rights reserved. The terms and conditions for the reuse of this version of the manuscript are specified in the publishing policy. For all terms of use and more information see the publisher's website.

This item was downloaded from IRIS Università di Bologna (<https://cris.unibo.it/>)

**When citing, please refer to the published version.**

1 *Acynodon adriaticus* from Villaggio del Pescatore (Campanian of Italy): anatomical  
2 and chronostratigraphic integration improves phylogenetic resolution in  
3 Hylaeochampsidae (Eusuchia)

4  
5 MUSCIONI MARCO<sup>1†</sup>, ALFIO ALESSANDRO CHIARENZA<sup>2†</sup>, MASSIMO DELFINO<sup>3, 4</sup>,  
6 MATTEO FABBRÌ<sup>5</sup>, KEVIN MILOCCO<sup>1</sup>, FEDERICO FANTI<sup>1</sup>

7 <sup>1</sup> *Dipartimento di Scienze Biologiche, Geologiche e Ambientali, Alma Mater Studiorum, Università*  
8 *di Bologna, via Zamboni 67, 40126 Bologna, Italy*

9 <sup>2</sup> *Grupo de Ecoloxía e Bioloxía Animal, Centro de Investigación Mariña, Universidade de Vigo,*  
10 *Vigo, 36310, Spain; ORCID: <https://orcid.org/0000-0001-5525-6730>*

11 <sup>3</sup> *Dipartimento di Scienze della Terra, Università di Torino, Via Valperga Caluso 35, 10125, Turin,*  
12 *Italy; ORCID: <https://orcid.org/0000-0001-7836-7265>*

13 <sup>4</sup> *Institut Català de Paleontologia Miquel Crusafont, Universitat Autònoma de Barcelona, Edifici*  
14 *ICTA-ICP, Carrer de les Columnes s/n, Campus de la UAB, 08193, Cerdanyola del Vallès,*  
15 *Barcelona, Spain*

16 <sup>5</sup> *Negaunee Integrative Research Center, Field Museum of Natural History, Chicago, IL, USA*

17 †These authors contributed equally to this work.

18 **e-mail:** [a.chiarenza15@gmail.com](mailto:a.chiarenza15@gmail.com); [alfio.chiarenza@uvigo.es](mailto:alfio.chiarenza@uvigo.es); [federico.fanti@unibo.it](mailto:federico.fanti@unibo.it);

19  
20 **Keywords**

21 Crocodylomorpha; Systematics; Bayesian; Maximum Parsimony; Cretaceous; Tethys;

22

23

24

25 ABSTRACT

26 The hylaeochampsid crocodylomorph *Acynodon adriaticus*, from the uppermost Cretaceous  
27 ‘Villaggio del Pescatore’ site, belongs to an early diverging lineage in Eusuchia. Here an additional  
28 specimen, MCSNT 57031, is osteologically and osteohistologically described in detail. After  
29 integrating this morphological information together with the recent chronostratigraphic recalibration  
30 of the site to the lower–middle Campanian, the tip-dated Bayesian phylogenetic analysis recovers this  
31 taxon in a monophyletic clade with the Spanish *Acynodon iberoccitanus*. Conflicting results from the  
32 maximum parsimony analyses and discussion on the intraspecific variability between the specimens  
33 assigned to *A. adriaticus* highlights the need for a detailed morphological description and integration  
34 with an updated phylogenetic scaffold, in order to resolve the monophyly of the genus *Acynodon* and  
35 the relationships of these branch of early diverging eusuchians. The curious discrepancy between  
36 morpho- and osteo-skeletal maturity suggest unique ecomorphological adaptations in this Campanian  
37 crocodylomorph.

38

## 39 1. Introduction

40 The Villaggio del Pescatore Lagerstätte (VdP hereafter), located in the municipality of Duino-  
41 Aurisina, Trieste (NE Italy), is a world-renown paleontological site due to its well-preserved  
42 Cretaceous vertebrate remains, standing out in the European palaeontological landscape (Chiarenza  
43 et al., 2021). In addition to the famous hadrosauroid *Tethyshadros insularis* (Dalla Vecchia, 2009;  
44 Chiarenza et al., 2021), remains of the small hylaeochampsid crocodylomorph *Acynodon adriaticus*  
45 were described from this site (Delfino et al., 2008a). *Acynodon* exhibits an overall bizarre morphology  
46 in comparison to other eusuchians, including a brevirostrine cranial condition: the skull is broadly  
47 similar to that of small alligatoroids (Brochu, 2010) although with larger and ‘molariform’ dentition.  
48 Given the bizarre morphology, fully reflective with the peak ecomorphological variation recently  
49 reported for Cretaceous crocodylomorphs by Stubbs et al. (2021), a stable phylogenetic placement of  
50 *Acynodon* in Eusuchia has been problematic (Rio and Mannion, 2021). *Acynodon* was previously  
51 considered as an example of ‘archaic’ alligatoroid, one of the oldest and most primitive  
52 representatives of the entire Globidonta (Santonian–Campanian) (Buscalioni et al., 1997; Brochu,  
53 2003; Martin, 2007; Brochu, 1999, 2001, 2003; Delfino et al., 2008a; Delfino et al., 2008b). However,  
54 recent phylogenetic analyses place this group outside Crocodylia in the clade Hylaeochampsidae,  
55 with conflicting results regarding the monophyly of the genus (Brochu, 2011, 2012; Brochu et al.,  
56 2012; Jouve et al., 2019; Martin et al., 2014, 2016; Ristevski et al., 2020; Blanco, 2021). *Acynodon*  
57 includes three known species: *A. adriaticus*, only known from the VdP site in Italy, *A. iberoccitanus*,  
58 with referred material from Spain, southern France and Romania (with remains from these latter two  
59 countries represented by multiple, fairly complete crania), and *A. lopezi* based on isolated teeth found  
60 in Spain (Buscalioni *et al.* 1997). Other occurrences of this genus come from several European  
61 locations (Blanco et al., 2020; Delfino et al., 2008a; Puértolas-Pascual et al., 2020): Muthmannsdorf  
62 (Austria), La Cabaña in Asturias (Spain), Chera (Spain), Els Nerets (Spain), Quintanilla del Coco  
63 (Spain), Laño (Spain), Arén (Spain), Masecaps (France), Quarante (France), Fox-Ampoux (France),  
64 Hațeg Basin (Romania) and VdP (Italy). Only *A. adriaticus* and *A. iberoccitanus* have been analysed

65 in a phylogenetic context (being the material referred to *A. lopezi* not informative enough). In a  
66 context of phylogenetic uncertainty (among others, Blanco, 2021; Martin et al., 2020; Narváez et al.,  
67 2016; Rio and Mannion, 2021), the revised chronostratigraphy of the VdP site (Chiarenza et al.,  
68 2021), type and only locality of *A. adriaticus*, offers a unique opportunity to test the phylogenetic  
69 implications of the temporal recalibration of this fossil bearing site.

70 This study focuses on *Acynodon adriaticus* with a comprehensive analysis of all skeletal  
71 remains ascribed to this taxon from the VdP site, discussing its age and taphonomy. Specifically, a  
72 nicely preserved individual, MCSNT 57031 (Fig. 1), assigned to the genus *Acynodon* by Delfino and  
73 Buffetaut (2006), conservatively considered as *Crocodylia* indet. by Delfino et al. (2008) due to the  
74 lack of definitive autapomorphies, is herein extensively described. Here we parsimoniously refer  
75 MCSNT 57031 to *A. adriaticus* by providing an accurate anatomical description of the specimen,  
76 followed by osteohistological analysis and consideration of the palaeobiology of *A. adriaticus*. We  
77 furthermore integrate these new anatomical and chronostratigraphic information in a combined  
78 framework to improve the resolution of the genus *Acynodon* (the less inclusive clade including  
79 *Acynodon adriaticus* and *A. iberoccitanus*).

80

## 81 **2. Institutional abbreviations**

82 MCSNT, Museo Civico di Storia Naturale in Trieste, Italy

83 MGGC, Museo Geologico Giovanni Capellini in Bologna, Italy

84

## 85 **3. Methods**

### 86 *3.1 Specimens*

87 All crocodylian remains from the VdP were collected between 1996 and 1999 (*see* Table 1)  
88 and are currently housed at the Museo Civico di Storia Naturale in Trieste (MCSNT). Specimens  
89 were prepared with a chemical dissolution technique consisting in selective matrix removal with

90 multiple formic acid baths. For this study, measurements and photographs were obtained *ex-novo* and  
91 compared with available prior measurements used in other publications (e.g. Delfino et al., 2008).  
92 The anatomical illustrations were preliminarily made using a microscope with integrated *camera*  
93 *lucida* (Leica DM 2500 P petrographic microscope with a ProgRes CFscan camera adapter),  
94 subsequently assembled with Adobe Photoshop 2020. Thin sections of rib fragments and dorsal  
95 osteoderms from MCSNT 57031 were prepared for osteohistological study and are housed in Bologna  
96 (access number MGGC 22304, 22305, 22306).

97

### 98 *3.1.1 New specimens assigned to Acynodon adriaticus and discussed in this study*

99 **MCSNT 57031**: ventrally exposed, articulated, sub-complete specimen (main focus of this study;  
100 Fig. 1); Initially described by Delfino and Buffetaut, 2006.

101 **MCSNT 21.S239-1.0.22 (57248a)**: six well-preserved osteoderms, three of them in partial overlap  
102 (Fig. 2A). The larger ones, measured at their longer axis, are 22.8 mm, 24.5 mm, and 27 mm long  
103 respectively. These osteoderms show two low keels, one straight and the other concave and larger,  
104 comparable to the condition described in the paratype by Delfino et al. (2008).

105 **MCSNT 57245**: an isolated, well-preserved robust crocodylian rib laying on the flat surface of a larger  
106 matrix slab with other unidentified bone fragments. The tuberculum is shorter than the capitulum and  
107 has a larger articular surface. The rib progressively thickens distally and has a wide costal cartilage  
108 articular surface (Fig. 2B).

109 **MCSNT 21.S239-1.0.22 (57248b)**: three small osteoderms and two robust ribs in association, both  
110 showing shorter and stouter tubercula than capitula, with wider articular surfaces (Fig. 2C). The  
111 shorter rib measures 46.7 mm in length and lacks its distalmost portion; the longer one measures 57.2  
112 mm, appears to be complete and gradually thickens at its distal end, revealing a large costal articular  
113 surface.

114

115 *3.1.2 Specimens assigned to Crocodylomorpha indet.*

116 **MCSNT 57033:** a ~4 cm long unidentified small reptile bone, possibly a rib, exposing its sagittal  
117 section on the surface of a small laminite fragment (Fig. S1A).

118 **MCSNT 57035:** a ~5 cm long bone element exposed on a calcareous slab with an ornamented surface,  
119 here identified as a ventrally exposed crocodylian mandibular symphysis (Fig. S1B).

120 **MCSNT 57036:** a ~2 cm anteroposteriorly long vertebra, possibly a fragmented cervical, three-  
121 dimensionally prepared out of the matrix (Fig. S1C).

122 **MCSNT 57037:** an almost unrecognizable smooth bone fragment hardly visible on a small matrix  
123 slab associated with other indeterminate vertebrate fossil material, previously tentatively identified  
124 as a fragmented ventral osteodermal surface (Fig. S1D).

125

126 *3.2 Stratigraphy and age*

127 The VdP site is located near a dismissed quarry in the municipality of Duino Aurisina, Trieste,  
128 Italy (Fig. 3). The overall geological setting of the site and surrounding areas, including key  
129 information on facies analysis, sedimentology, paleontology, and isotope-based stratigraphy, has  
130 been described in detail in the literature (Tarlao et al., 1993, 1995; Attura, 1999; Palci, 2003; Dalla  
131 Vecchia, 2008, 2009; Chiarenza et al., 2021; Consorti et al., 2021), with a recent redescription and  
132 re-evaluation documented in Chiarenza et al. (2021). The VdP deposits originated at the northern  
133 margin of the Adriatic Carbonate Platform system (AdCP): in the area, the Upper Cretaceous to  
134 lowermost Paleocene interval is represented by two informal units, the Aurisina formation and the  
135 Cretaceous/Palaeogene (K/Pg) bearing Liburnian formation (or by their equivalent synonyms along  
136 the adjacent Slovenian units [*see* Jurkovšek et al., 2016]). From a sedimentological perspective, the  
137 site is included in the Aurisina formation and is represented by sharp *facies* variations from open  
138 marine, shallow-water limestones to organic-rich rhythmites, which interbed with breccias that  
139 accumulated as underwater bodies by subaqueous, density-driven, sedimentary flows. Each  
140 identifiable lamina consists of micro-couplets made by a millimetric-thick, dark colored, organic-rich



141 lamina superimposed to a light lamina made of carbonate mud. Given an overall thickness of ~10 m  
142 and a thickness of each couplet ranging from 1 to 2.5 cm, the ‘*laminites*’ lens was estimated to  
143 represent a time interval of 4–10 kyrs (Arbulla et al., 2006). However, recent surveys at the site have  
144 documented how rhythmites and breccia bodies are folded by syn-depositional slumping and  
145 deformed by wet-sediment normal faults, thus largely reducing the estimated depositional length to  
146 few thousand kyrs (Chiarenza et al., 2021). Relevant to our comprehension of the genus *Acynodon*, a  
147 recent revision of the fossil content of the site has restricted the dating of the fossil interval to the  
148 lower-middle Campanian (81.5–80.5 Ma) based on the vertical distribution of the benthic  
149 foraminifera assemblage and calibrated with strontium isotopes stratigraphy (Frijia et al., 2015;  
150 Chiarenza et al., 2021). From a stratigraphic perspective, specimen MCSNT 57031 represents the  
151 lowermost occurrence of *A. adriaticus* at the site, being collected at the onset of the organic-rich  
152 rhythmites. All other elements discussed in this paper are confined in a very restricted interval made  
153 of a single, syn-depositional, slumped set of rhythmites. Remarkably, this interval also includes  
154 crustaceans, fish, coprolites, and the fully articulated specimens of the hadrosauroid dinosaur  
155 *Tethyshadros insularis* (see Chiarenza et al., 2021). Taphonomic and sedimentological parameters  
156 support a rapid genetic process for this interval, thus hinting to the presence of a single eusuchian  
157 taxon at the site.

158

### 159 3.3 Taphonomy

160 Slumped rhythmites at the VdP raise crucial questions concerning the taphonomy of the site,  
161 including the preservation of vertebrate remains (i.e.: dinosaurs, pterosaurs, crocodiles, fish) in  
162 dysoxic-anoxic bottom waters in marginal-marine settings. Prior to this study, a complete survey of  
163 crocodylomorph material from the VdP site was never addressed, and very little was known on the  
164 precise stratigraphic occurrence of crocodylian remains within the relatively small fossil-bearing area.

165 Therefore, for this study, a comprehensive survey of fossil material housed at the MCSNT was  
166 undertaken, coupled with a detailed analysis of all available quarry reports and associated  
167 photographic material of extractive campaigns between 1996 and 2020 (Dalla Vecchia, 1999; F.  
168 Bacchia, pers. comm. 2022). In addition, we used Unmanned Aerial Systems (UAS) and Vehicles  
169 (UAV) and related processing technologies to produce the most accurate and up-to-date quarry map  
170 (Fig. 3A-C) for the VdP site, a framework into which geological and paleontological data could be  
171 precisely included (Fig. 3D). Using these elements we produced an up-to-date list of crocodylian  
172 specimens (*see 3.1*) and were able to relocate each specimen into the stratigraphic setting of the main  
173 quarry area. Our data indicate that the occurrence of crocodylian remains is limited to very precise  
174 stratigraphic intervals, each represented by a single, slumped, approximately 1.5 meter thick, set of  
175 laminae (Fig. 3D). These intervals contain the vast majority of fossil remains from the site. Specimen  
176 MCSNT 57031 is the lowermost occurrence of crocodylians at the site, found in the proximity of an  
177 articulated but poorly preserved individual of *Tethyshadros insularis* (SC 57026). The type specimen  
178 of *A. adriaticus* (MCSNT 57248) and most isolated crocodylian elements were collected from the  
179 same slump that preserved the type specimen of *T. insularis* (SC 57021) and other nicely preserved  
180 and articulated dinosaur remains (SC 57022). Finally, a single isolated bone assigned to an  
181 undetermined crocodylian was collected from a third slump in the proximity of a fully articulated  
182 skeleton of *T. insularis* (SC 57247) and to other, still *in situ*, articulated dinosaur remains.  
183 Remarkably, at the VdP site, large and fully articulated vertebrates are found in association with  
184 recurrent fish and crustacean remains: this, coupled with the documented sharp facies variation (open  
185 marine limestone to slumped, organic-rich rhythmites interbedded with breccias), rise questions on  
186 the depositional processes that led large terrestrial taxa and minute, both freshwater and marine  
187 species, to be rapidly buried into anoxic, shallow marine settings.

188

### 189 3.4 Osteohistological sampling

190 We sampled the 6<sup>th</sup> dorsal rib and a loose osteoderm fragment (presumably cervical) for  
191 osteohistological analyses, in order to investigate the ontogenetic stage of MCSNT 57031. Although  
192 long bones have been shown to have a better-preserved growth record, and, therefore, to be more  
193 appropriate for quantitative extrapolation of growth strategies and life history, these elements were  
194 inaccessible in our sample for curatorial reasons. Furthermore, dorsal ribs and osteoderms have been  
195 demonstrated to be excellent skeletal elements for an effective and reliable ontogenetic assessment  
196 across tetrapods, and, more specifically, for non-avian archosaurs (Erickson and Brochu, 1999; de  
197 Ricqlès et al., 2003, 2003; Parker et al., 2008; Scheyer and Sander, 2009; Witzmann, 2009; Witzmann  
198 and Soler-Gijón, 2010; Scheyer and Desojo, 2011; Woodward Ballard et al., 2011; Cerda and Desojo,  
199 2011; Taborda et al., 2013; Woodward et al., 2014; Ponce et al., 2017; von Baczko et al., 2019). The  
200 thin sections were prepared following the protocol by Chinsamy and Rath (1992), reaching a final  
201 thickness of 50–70 microns in the samples that were then analyzed with a Leica DM 2500 P  
202 petrographic microscope. Photographs of the thin sections were taken with a ProgRes Cfscan camera.  
203 Inference of skeletal maturity follows recently proposed nomenclature by Griffin et al. (2021)

204

### 205 3.5 Phylogenetic analyses

206 We scored the holotype of *Acynodon adriaticus* (MCSNT 57248) and MCSNT 57031 as  
207 independent Operational Taxonomic Units (OTUs) performing a maximum parsimony and time-  
208 calibrated Bayesian phylogenetic analyses. We used the phylogenetic data matrix published by  
209 Blanco (2021), an update of the dataset from Narváez et al. (2016) and originally published by Brochu  
210 and Storrs (2012). This matrix does not include the Spanish hylaechampsid *Unasuchus* (Brinkmann,  
211 1992), since the limited amount of material referred to the taxon (and the interpretative drawings  
212 reported in the literature) allows a minimal amount of scoring in the Blanco's (2021) matrix.  
213 Similarly, the Turkish taxon *Turcosuchus* (Jouve et al., 2019) is based on fragmentary material with  
214 limited characters scorable in Blanco (2021). A total of 85 out of 189 characters and 31 out of 189

215 characters were scored for MCSNT 57248 and MCSNT 57031 respectively in Mesquite 3.70  
216 ([www.mesquiteproject.org](http://www.mesquiteproject.org)), for a total of 109 OTUs (Data S1).

217 Characters were treated as unordered and equally weighted. Maximum Parsimony analyses  
218 were computed in TNT 1.5 beta (Goloboff et al., 2008), using a ‘New Technology’ search, with Sect  
219 Search, Ratchet, Drift, and Tree Fusing algorithms, and 10 random addition sequences (Chiarenza et  
220 al., 2020). A thorough exploration of tree space for obtaining strict consensus and majority rule trees  
221 was computed on the trees held in RAM via a ‘Traditional Tree Bisection-Reconstruction (TBR)  
222 Branch-Swapping’ method and both Bootstrap and Bremer support was calculated using standard  
223 absolute frequencies for 1000 replicates. The analysis recovered 9 trees with best step length score of  
224 807. Notably, the use of TBR after the ‘New Technology’ search further explores the tree space  
225 ([Barrett et al., 2014](#); [Raven and Maidment, 2018](#)). Notably, while this procedure differs from those  
226 described in [Blanco \(2021\)](#), [Brochu \(2011\)](#), [Narváez et al. \(2016\)](#) and [Puértolas-Pascual et al. \(2020\)](#),  
227 it generated similar general tree topologies, although with different steps and support values.

228 For the Bayesian analysis, the same nexus file used for the Maximum Parsimony analyses was  
229 expanded following the optimization criteria for ‘Morphological Clock Analyses’ (Lee et al., 2014)  
230 in MrBayes 3.2.7. OTUs’ age was matched using midpoint age constraints available in Mannion et  
231 al., (2019) and updated following recent chronostratigraphic updates on fossil crocodylian bearing  
232 formations (e.g. Chiarenza et al., 2021). Age values and tips in tree were paired using the function  
233 ‘`phylo_check`’ from the package ‘`palaeoverse`’ (Jones et al., 2023) in R version 4.1.3. The MrBayes  
234 script encoded the use of a gamma parameter for modelling uniform rate variation across traits, an  
235 uncorrelated relaxed clock for modelling rate variation across branches was used instead (`igr`) of  
236 autocorrelated, relaxed clock or a strict clock following Lee et al., (2014). The convergence of all  
237 independent runs, together with stationarity were assessed using TRACER v.1.7.1, assuming  
238 significance of effective sample size (ESS) for each parameter when  $\geq 200$  (Rambaut et al., 2018).  
239 MrBayes script is included as Data S2. Tree topologies were explored in FigTree v1.4.4. Time-  
240 calibrated Bayesian tree was plotted for showing stratigraphic ranges of the tips using the R package

241 'strap' by Bell and Lloyd (2015), which was also used to calculate values of stratigraphic congruence  
242 of different tree outputs compared to randomly generated trees using the Stratigraphic Consistency  
243 Index (SCI).

244

## 245 **4. Results**

### 246 *4.1. Systematic Paleontology*

247 **Crocodylomorpha** Hay, 1930 *sensu* Nesbitt, 2011

248 **Neosuchia** Benton and Clark, 1988

249 **Eusuchia** Huxley, 1875 *sensu* Brochu, 2003

250 **Hylaeochampsidae** Andrews, 1913

251 *Acynodon* Buscalioni *et al.* 1997

252 *Acynodon adriaticus* Delfino *et al.* 2008

253

### 254 *4.2 Description of MCSNT 57031*

#### 255 **Skull**

256 The ventrally exposed cranium (Fig. 4) is roughly 15 cm long, only partially preserved, and  
257 obliterated by the slab matrix on its dorsal margin. Based on visible elements (Fig. 4B) it appears to  
258 be roughly 80% of the holotype in anteroposterior size (Fig. 5). No maxillary nor premaxillary teeth  
259 are visible. Part of the rostral region, although fragmentary, is preserved and corresponds to the palatal  
260 portion of the right maxilla (Fig. 4). Very little is preserved of the posterior region of the skull: a  
261 wide, subrectangular articular surface (Fig. 4) may represents the ventral portion of the quadrate  
262 condyle. However, given the fragmentary preservation, such element may also be the articular glenoid  
263 fossa, exposed dorsally due to a rotation of 180°.

264 The distal section of the right dentary is three-dimensionally preserved, exhibiting clear  
265 ornamentations on the labial surface arranged as longitudinal grooves (Fig. 6). The suture with the

266 splenial is located on a deep groove on the ventromedial surface of this distal portion of the  
267 mandibular ramus (Fig. 4B). The splenial is well preserved, showing three aligned foramina (Fig. 6).  
268 The slab margin is obscured by a protective layer of resin, thus precluding additional observations on  
269 the mandible and skull elements. The angular, surangular and articular bones are heavily fragmented  
270 and hardly distinguishable. The right retroarticular process is partially damaged but better preserved  
271 than the left one, at least in its general outline (Fig. 4). From the posterior end of the retroarticular  
272 process to the preserved distal end of the dentary, the right mandibular ramus is 132 mm long and  
273 around 10 mm thick dorsoventrally in its distal, less deformed section. The left mandible is  
274 represented only by small, hardly identifiable proximal fragments, most likely the angular and  
275 articular. One fragment preserves the ornamented surface texture (Fig. 6), with the relatively large  
276 pits morphologically similar to those observed on the angular and surangular surfaces of the holotype.

277

#### 278 **Axial skeleton**

279 The preserved cervical vertebrae are lateroventrally exposed on their left side (Fig. 7): centra  
280 show a markedly procoelic condition. Five articulated middle cervical vertebrae, complete with  
281 centra, neural arches and cervical ribs are identified and tentatively interpreted as cervicals 3–7, with  
282 an anterior neural spine and a few overlapping or nearby fragments corresponding to cervical c2 or  
283 c1+c2, and a posteriorly disarticulated tall neural spine probably referable to c8. Given the estimated  
284 number of eight total cervical vertebrae in the holotype (Delfino *et al.* 2008), the series could be  
285 partially overlapped with the holotypic cervical one. Centra are twice anteroposteriorly long as  
286 dorsoventrally high. Centra are mediolaterally wide with relatively short and lateroventrally directed  
287 parapophyses. The putative c2 centrum is partially lateroventrally rotated, exposing either a convex  
288 anterior articular facet, a ventral tuberosity or a blunt hypapophysis. At least 7 cervical ribs are  
289 exposed on the surface of the slab, with three well preserved left ribs associated with cervicals 3–5.  
290 Ribs have short tubercula and capitula, and they are hatchet-shaped in overall morphology, with a  
291 smooth surface and with curved and relatively thick inferior margins. Neural arches are apparently

292 not articulated to each other in cervicals 4–6, and in c5 and c6 they are clearly unfused from their  
293 centra, exhibiting open neurocentral sutures (Fig. 7). Both zygapophyses are clearly recognizable in  
294 c3, a single c2 postzygapophysis is still articulated to c3 and traces of a prezygapophysis are  
295 potentially visible in c4. The c8 neural spine is clearly detached from its arch. Overall, the  
296 morphology of the more anterior neural spines is flatter and more anteroposteriorly elongated,  
297 gradually becoming proportionally taller and narrower in c5 and c6, with the supposed c8 spine being  
298 the tallest of the preserved series, bearing also a distal anteroposterior expansion. An additional  
299 vertebral centrum, possibly one of the first dorsal vertebrae, is partially preserved posteriorly to the  
300 last cervical neural spine, apparently rotated by almost 180°.

301

## 302 **Ribs**

303 Assessing the exact number of preserved ribs is challenging due to the fragmentary nature of  
304 the specimen. At least three partial ribs can be recognized on the left side of the animal, located  
305 between the bend of the cervical series and the dorsal patch of osteoderms, whereas on the right side,  
306 at least nine ribs or partial ribs are preserved (Fig. 8). Their morphology is characterized by a wide  
307 anteroposterior expansion along their diaphyses, therefore presumably appearing as a flattened oval  
308 shape or eccentrically D-shaped section. The distal epiphysis is preserved in some ribs, appearing to  
309 be blunter and more rectangular in their outline in longer posterior ribs than in the anterior ones,  
310 consistent with the attachment for cartilage portions connecting the sternal ribs or gastralia. At least  
311 three small, elongated structures overlapping with the unidentified clusters of dark bone portions in  
312 the abdominal region of the specimen might represent small fragments of gastralia or other sternal  
313 ribs (Fig. 8). The dark amorphous mass that partially engulfs them, already described by Delfino  
314 (2008) as a “uniformly vermicular surface”, most likely is here identifiable as a cluster of small lateral  
315 or ventral osteoderms exposed on their visceral surface, heavily overlapped and crushed together.

316

## 317 **Pectoral girdle**

318           The right coracoid is preserved close to the right humerus and partially overlapped by a  
319 narrow-elongated bone, here interpreted as the interclavicle (Fig. 9). The margin of its enlarged distal  
320 end appears to be slightly damaged and its proximalmost portion not properly visible. The left  
321 coracoid is either not preserved or represented by some fragments located anteriorly to the left  
322 humerus. The interclavicle has an enlarged, weakly plate-shaped anterior end. Toward its posterior  
323 margin, a short longitudinal keel is visible (Fig. 9). A partially exposed element overlapped by the  
324 right coracoid most probably represents the ventrally exposed right scapula. Its shape is consistent  
325 with the holotypic right scapula, with subparallel dorsal and ventral margin of the distal portion, but  
326 the bad preservation and partial damage in this area prevents a proper description of its morphology  
327 at its distalmost process. Given the relevance and direct phylogenetic implication of the scapular  
328 blade morphology in crocodylians (*see Brochu and Storrs, 2012*), we prefer not to define (and score)  
329 the morphology of this anatomical trait. The heavily damaged bone between the right scapula and the  
330 left humerus can be tentatively referred as the left scapula. The more anterior position of the entire  
331 pectoral girdle in the fossil, in relation to the ribs and axial skeleton, suggests an anteriorward slippage  
332 of the forelimb-girdle complex from their *in vivo* position.

333

#### 334           **Right forelimb**

335           Except for a few elements of the manus, the entire right forelimb is exquisitely preserved,  
336 although slightly disarticulated. The humerus is ventrally exposed and displays a prominent concave  
337 deltopectoral crest with a well-defined apex (Figs. 10, 11), becoming a low longitudinal crest in its  
338 proximoventral portion; the deltopectoral crest runs almost up to the distal epiphysis, with a rough  
339 apical surface texture reminiscing of a fibrous surface. The proximal epiphysis is not sharply rotated  
340 relatively to the distal epiphysis (as described in character 303 by Rio and Mannion 2021). A  
341 relatively large, saddle-like surface lies between the well-developed radial and ulnar condyles, the  
342 latter being larger and more laterally prominent. The articular surface of the distal epiphysis exhibits



343 a rough surface, indicating the exact location of the articular cartilage. An interesting detail is the  
344 osteoporotic-like bone tissue on the distal condyles (Fig. 12).

345 The right radius and ulna are robust, medially exposed, parallel to each other (slightly offset  
346 from their anatomical position) and near to the distal end of the humerus. They appear to be still  
347 articulated at their distal end and only slightly disarticulated proximally. The olecranon process of  
348 the ulna is approximately round, the proximal epiphysis is the thickest portion of the bone, the  
349 diaphysis gradually becomes thinner towards the distal epiphysis, which is probably missing a small  
350 portion, or it is not completely ossified. The radius is distally as thick as the ulna, with well developed,  
351 wide epiphysis. The epiphyses of both the radius and ulna show a similar osteoporotic bone tissue as  
352 in the distal humerus (Fig. 11).

353 The carpus seems to be complete, and all its elements are lying in anatomical position. The  
354 large radiale and ulnare are well preserved with the epiphyseal surfaces showing osteoporotic-like  
355 conditions as in the humerus, radius, and ulna (Fig. 12). A carpal element distal to the pisiform seem  
356 to be partially fragmented into two separate elements. While the fragmentary nature of these –  
357 partially still embedded in matrix – elements prevent a confident identification, one of this may  
358 represent the central carpal [centrale *sensu* [Gregorovičová et al., \(2018\)](#); Fig. 12B]. A few bone  
359 fragments scattered between the zeugopodium and the carpus may be coming from the anterior  
360 proximal portion of the two larger carpals or from the anterior distal end of the radius and/or ulna.  
361 The matrix obscures most portions of these elements. Three metacarpals are well preserved,  
362 tentatively identifiable as metacarpals I, II and III due to their relative arrangement and position to  
363 the carpus. Other two bone elements, possibly the other two metacarpals or phalanges, can be found  
364 below these elements. All metacarpals show an even more pronounced epiphyseal bone porosity and  
365 irregular surface than every previously mentioned element (Fig. 12). Five phalanges and two closely  
366 placed unguals are preserved. The smaller ungual phalanx is found against the metacarpal III, whereas  
367 the larger one, relatively big in comparison to the overall forelimb proportions, is characterized by a  
368 deep lateral groove, with a short flexor tubercle and pronounced dorsal and ventral process.

369 In adult crocodylians the carpus has a highly reduced number of ossified elements, with living  
370 representatives (e.g. Alligatoridae) having four elements [*Alligator mississippiensis*, (Müller and  
371 Alberch, 1990), *Caiman yacare* (Lima *et al.*, 2011), *Melanosuchus niger* (Vieira *et al.*, 2018)].  
372 *Acynodon* is therefore expected to reflect a similar condition: in this specimen however, although four  
373 major elements are clearly identifiable (Figs. 10, 12), a higher number may be present but obscured  
374 by and preservation of these elements.

375

### 376 **Left forelimb**

377 Of the left forelimb, the humerus, radius, ulna, the ulnare, and four (possibly five) manual  
378 elements are preserved (Fig. 13). The humerus, radius and ulna are badly fragmented, and the bone  
379 surface in all of them is not as well preserved as in the right forelimb. The humerus is broken halfway  
380 along its proximodistal length. The radius and ulna are overlapping along their proximodistal length  
381 and appear broken at their diaphysis. What seems to be a heavily damaged radiale partially overlaps  
382 the distal ulnar epiphysis. Up to five other elements are located distally to the radiale including two  
383 possible metacarpals or a metacarpal and a carpal. Given their morphology and size, they are here  
384 interpreted here as an ulnar carpal, two metacarpals and two phalanges (Fig. 13).

385

### 386 **Osteoderms**

387 Many osteoderms are preserved in MCSNT 57031 (Fig. 1). A few oval, cervical osteoderms  
388 are preserved in ventral view around the cervical area. The largest and most articulated osteoderm  
389 cluster is located dorsally to the rib cage. Despite the overall orientation of the specimen (lying on its  
390 ventral side), the entire osteoderm series is dorsally exposed so that the dorsal left rows are visible.  
391 Single osteoderms of this area are partially overlapping their neighboring elements on their right and  
392 posterior end. This arrangement suggests a 180° rotation of the entire dorsal and lateral osteoderm  
393 armor. Ventrally to the anterior elements, however, a smooth surface may in fact represent the  
394 somewhat smoother ventral surface of the osteoderms from the row of the right side. Following this

395 interpretation, the whole paravertebral shield would have been affected by a sharp lateral folding  
396 along its parasagittal axis. Morphologically, dorsal osteoderms are squared in overall shape,  
397 proportionally large mediolaterally and with deep circular pits and grooves surrounded by tall keels  
398 on their dorsal surfaces (Fig. 14A). The second anteriormost osteoderm is the best preserved one and  
399 displays a radial arrangement of the dorsal ornamentation (Fig. 14B). The majority of other  
400 osteoderms exhibit a dorsal tubercular keel running posteriorly and diagonally to the osteoderm  
401 quadrangular outline, a feature consistent with the ornamentation of the outer lateral rows of dorsal  
402 osteoderms of the paratype MCSNT 57032 described by Delfino *et al.* 2008, although they display a  
403 much smoother surface. The previously mentioned dark and smooth mass (Fig. 8) located in the  
404 abdominal region of the specimen may represent a second cluster of osteoderms. In this roughly  
405 polygonal outline, we recognized two main areas: a dorsal one, characterized by a smooth continuous  
406 surface, and a ventral amorphous osteoderm mass, with a rougher pattern vaguely reminiscent of  
407 black flakes at its margins.

408

#### 409 *4.3 Osteohistology*

##### 410 **Dorsal rib (6th)**

411 The cross section of the dorsal rib appears oval in shape (Figure 15A). Trabecular bone is  
412 present in the medullary cavity, making the transition from the center of the section to the cortex  
413 gradual and characterized by intense remodeling (Figure 15A). The primary bone tissue is composed  
414 of lamellar bone (Figure 15B-C). Primary vascularization is very rare and sparse, but present, and is  
415 mainly longitudinal in orientation. Large, secondary osteons are present in the inner third of the  
416 cortex, obscuring the early growth record. 31 Lines of Arrested Growth (LAGs) are present; annuli  
417 are commonly present. An External Fundamental System (EFS) is absent.

418

##### 419 **Osteoderm**

420 The primary bone tissue composing the cortex is constituted by lamellar bone (Figure 15D-  
421 E). Primary vascularization is scarce, but present with a longitudinal orientation. Zonation is present  
422 in the preserved primary cortex: 15 LAGs can be counted. Cancellous bone, erosional cavities, and  
423 haversian systems obscure the majority of the inner cortex, as generally observed in osteoderms  
424 among pseudosuchians. The lower number of LAGs recovered in the cortex of the osteoderm in  
425 comparison to the count in the dorsal rib is therefore explained by the overprinting of the early growth  
426 record by bone remodeling. An EFS is absent, although zonation tends to decrease and the primary  
427 vascularization becomes virtually absent towards the outer surface of the osteoderm.

428

## 429 5. Phylogenetics

430 The phylogenetic relationships of MCSNT 57031 and the holotype of *A. adriaticus* MCSNT  
431 57248 were tested with Maximum Parsimony and Bayesian analyses (Fig. 16). The maximum  
432 parsimony strict consensus of 9 trees (Fig. 16A, Fig. S2) is 807 steps long, with a Consistency Index  
433 of 0.305 and a Retention Index of 0.785. The strict consensus recovers both specimens assigned to *A.*  
434 *adriaticus* in a polytomy with *Hylaeochampsa vectiana* and *Iharkutosuchus makadii* [Bremer (decay)  
435 Index of DI = 1]. *Acynodon iberoccitanus* is found as sister group of this polytomy (DI = 2).  
436 *Shamosuchus djadochtaensis* and *Pietraroiiasuchus ormezzanoi* are found in a polytomy with the  
437 *Acynodon* + *Hylaeochampsa* clade (DI = 1). The Majority rule tree (Fig. 16B, Fig. S3) increases  
438 resolution in this ‘hylaeochampsid polytomy’ placing both specimens of *A. adriaticus* (bootstrap  
439 support of BS = 77%) as sister group of the clade including *H. vectiana* and *I. makadii* (BS = 100%),  
440 but breaking the monophyly of the genus *Acynodon*, since the Spanish eponym taxon *A. iberoccitanus*  
441 is found as sister taxon of the *Hylaeochampsa* + *A. adriaticus* clade (BS = 100%). According to this  
442 result, a synapomorphy of Hylaeochampsidae is the maxilla with a posterior process between the  
443 lacrimal and the prefrontal (character 128, state 2 of [Brochu and Storrs, 2012](#)). The synapomorphy  
444 defining the *Acynodon* + *Hylaeochampsa* clade is the presence of anterodorsally projected anterior

445 dentary teeth (character 48, state 1 of Brochu and Storrs, 2012). The *Hylaeochamposa* + *A. adriaticus*  
446 clade is defined by: a penultimate maxillary alveolus more than twice the diameter of the last  
447 maxillary alveolus (character 106, state 1 of Brochu and Storrs, 2012); a prefrontal longer than the  
448 lacrimal (character 130, state 1 of Brochu and Storrs, 2012); and a quadrate bearing a prominent,  
449 mediolaterally thin crest on its dorsal surface (character 179, state 1 of Brochu and Storrs, 2012).  
450 *Acynodon iberoccitanus* is diagnosed in this analysis by the unexposed supraoccipital on the dorsal  
451 surface of the skull table (character 160, state 1 of Brochu and Storrs, 2012).

452 The Bayesian analysis (Fig. 16C; Fig. S4) solves this paraphyletic ambiguity by placing *A.*  
453 *adriaticus* and *A. iberoccitanus* in a monophyletic clade, with a Posterior Probability (PP) value of  
454 80. The genus *Acynodon* is sister taxon of *I. makadii* (PP=60), and both form the sister group of *H.*  
455 *vectiana* (PP=91). This hylaeochampsid clade is sister group (PP=86) of a lineage including  
456 *Pietraroiasuchus ormezzanoi* and *Shamosuchus djadochtaensis* (PP=61). The phylogenetic topology  
457 found in the Bayesian analysis has as higher stratigraphic congruence (SCI=0.5–1 > 0.45; Fig. S5)  
458 than the strict consensus (SCI=0–0.45 > 0.48; Fig. S6) and the majority rule (SCI=0.5–1 vs 0.585;  
459 Fig. S7) trees from the maximum parsimony analysis.

460

## 461 **6. Discussion**

### 462 *6.1 Differences between MCSNT 57031 and Acynodon adriaticus holotype MCSNT 57248*

463 Based on overall measurements, MCSNT 57031 is smaller than the holotype MCSNT 57248 (Fig.  
464 17), but single elements show different degree of size disparity between the two specimens.  
465 Allometric growth of individual bones is common in crocodylians (Kramer and Medem, 1955;  
466 Dodson, 1975; Deeming and Ferguson, 1990), implying that measurements of single bones are  
467 inappropriate for precise body size estimations (Brochu, 1996), preventing a further discussion on  
468 speculative absolute estimates.

469 From an overall superimposition between the MCSNT 57031 lower jaw outline and the  
470 holotype, some differences emerge (Fig. 5). The holotype possesses a ~20% longer mandible  
471 compared to MCSNT 57031, suggesting a larger skull in this individual. The right mandibular ramus  
472 of MCSNT 57031 measures 123.4 mm in length, although it is distally incomplete. The maximum  
473 mediolateral width of the mandible, when considering from the right angular/surangular region to the  
474 highly damaged angular fragments of the left hemimandible, measures 98.5 mm. According to  
475 Delfino et al. (2008) the holotype skull is 155 mm long from the distal premaxilla to the posterior  
476 edge of the quadrate condyles and is 125 mm wide. Unfortunately, no longitudinal measurements of  
477 the ventrally exposed mandibular rami are provided in Delfino et al. (2008), but we provide an overall  
478 measurement of 165 mm in length. Although incomplete at the symphyseal region, the holotype  
479 mandible is roughly 24% longer than in MCSNT 57031. Intraspecific variability in skull proportions  
480 was documented in *Acynodon iberoccitanus* specimens ACAP-FX1 and ACAP-FX2 (Martin, 2007).  
481 While considering intraspecific variability a possibility, we consider such differences in available  
482 *Acynodon adriaticus* specimens as better explained by taphonomical damage and partial bone  
483 dislocation.

484 As mentioned above, when compared to the holotype, cervical centra in MCSNT 57031  
485 appear proportionally longer and more gracile, most likely due to differential preservation. Delfino  
486 et al. (2008) estimated an anteroposterior length of 17 mm for the holotypic c6 centrum. We measured  
487 the putative c6 centrum in MCSNT 57031 reporting the same measurement (17.2 mm long), thus  
488 comparable in anteroposterior length. In the holotype, the neurocentral sutures of all visible vertebrae  
489 are closed (Delfino et al., 2008a), suggesting developmental maturity at the time of death (Brochu,  
490 1996). Cervical vertebrae of MCSNT 57031 show detached neural arches from the respective centra  
491 along relatively smooth section-like fractures, most probably representing open neurocentral sutures  
492 (Fig. 7). Neurocentral sutures in the crocodylian axial skeleton follow a distinct caudal to cranial  
493 closure sequence during ontogeny, with the sutures in caudal vertebrae being fully closed in  
494 hatchlings, and closure of remaining sutures toward the cranium occurring progressively later.

495 Closure of the cranial-most sutures occurs relatively late in ontogeny and indicates the attainment of  
496 morphological maturity (Brochu, 1996). Without histological information, this trait in MCSNT 57031  
497 might be interpreted as a signal of developmental immaturity.

498 The bone surface on the epiphysis of long bones and manual elements in MCSNT 57031 is  
499 consistently osteoporotic, a condition not documented in the holotype. Similar but not identical traits  
500 are often linked to skeletal immaturity in tetrapods. This trait however affects a different region of  
501 the bone, and Tumarkin-Deratzian et al. (2006) demonstrated that little to no association was present  
502 between bone textures and either body size or skeletal maturity in *Alligator mississippiensis*, possibly  
503 due to the extremely plastic environment-induced developmental rates common to most crocodylians.  
504 This makes the porosities on MCSNT 57031 a weak immaturity signal if considered alone, although  
505 it is still widely used for other archosaurs, particularly of the avian lineage (Bennett, 1993; Carr, 1999;  
506 Chiappe and Göhlich, 2010; Chiarenza et al., 2020; Hone et al., 2016; Sampson et al., 1997). In  
507 contrast, the osteoarthropathy of unknown etiology reported by Huchzermeyer et al. (2013) in  
508 *Crocodylus niloticus* is not correlated to ontogenetic immaturity, and the reported humeral epiphyseal  
509 osteolytic lesions are somewhat similar to the condition described for MCSNT 57031. The  
510 pathological nature of the epiphyseal porosity discussed here should not be excluded.

511 Although not somatically mature, ontogenetic immaturity (juvenile ontogenetic stage) can be  
512 rejected in MCSNT 57031 based on osteohistological results. The amount of remodeling in the inner  
513 cortex of the dorsal rib, the high number of LAGs, and the decrease of spacing between them suggest  
514 that sexual maturity was probably reached in this individual (Fig. 15). These results contrast with the  
515 osteological observations suggesting an immature ontogenetic stage for MCSNT 57031. Although it  
516 is currently unclear why such mismatch between these observations is present, previous studies have  
517 shown how osteohistological analyses are generally preferable and more reliable than osteological  
518 observations (e.g. Griffin et al., 2021). Lack of closure for neurocentral sutures along the axial  
519 skeleton and porous epiphyses in the long bones have been previously observed in late ontogenetic  
520 stages in aquatic animals, such as marine reptiles: these were described as skeletal paedomorphosis

521 and suggested to be an adaptation to more aquatic ecologies (e.g. Motani et al., 2015; Rieppel, 1989).  
522 A paedomorphic overall skeletal morphology due to the potentially bizarre ecomorphology of  
523 *Acynodon adriaticus* is a possibility, although more data and observations are necessary to confirm  
524 this.

525

## 526 6.2 Phylogenetic implications of MCSNT 57031 for the phylogeny of *Acynodon*

527 Few morphological characters in MCSNT 57031 improved previous scorings of *A. adriaticus*  
528 material in the available character matrix. Character 26 in Brochu and Storrs (2012), related to the  
529 scapulocoracoid facet anterior to glenoid fossa and previously unscored in the holotype, is scored  
530 here from MCSNT 57031 as broad immediately anterior to glenoid fossa, and tapering anteriorly.  
531 Similarly, the olecranon process of the ulna (Character 29 in Brochu and Storrs, 2012) is scored as  
532 wide and rounded. The dentary is scored as gently curved in MCSNT 57031 (Character 50 in Brochu  
533 and Storrs 2012), a feature previously unscored from the holotype. The strict consensus from  
534 maximum parsimony analysis recovers a complete polytomy of the main groups of Eusuchia when  
535 the specimen MCSNT 57031 is added to the dataset, while when this OTU is inactive, the topology  
536 between the main eusuchian lineages is identical to that reported by Blanco (2021). This is probably  
537 due to the low proportion of diagnosable characters in this specimen of *A. adriaticus*.

538 On a purely morphological basis and under a maximum parsimony approach, the phylogenetic  
539 integration of the new scoring confirms the paraphyly of *Acynodon* as shown in several previous  
540 analyses (Brochu, 2011; Brochu, 2012; Brochu et al., 2012; Blanco, 2021; Martin et al., 2014, 2016;  
541 Jouve et al., 2019; Ristevski et al., 2020; Narváez et al., 2016). If confirmed, this may require the  
542 erection of a new genus, based exclusively on the material from VdP, but further reconsideration  
543 including a redescription of the other species included in *Acynodon*, at the light of several newly  
544 described characters of phylogenetic value, is strongly needed. In particular, a better scoring of the  
545 poorly preserved hylaeochampsids and the retrieval of new remains (above all *Hylaeochampsia*)



546 would be also recommended in order to properly reevaluate the phylogeny and therefore taxonomy of  
547 *Acynodon* as well as the phylogenetic position of Hylaeochampsidae and closely related taxa within  
548 Eusuchia.

549 We remark that the chronostratigraphic re-evaluation of the age of VdP to the early–middle  
550 Campanian improves stratigraphic congruence and sets the specimens of *A. adriaticus* as  
551 chronologically older and stratigraphically overlaid by the range of *A. iberoccitanus*. Furthermore,  
552 the Bayesian analysis re-establishes the monophyly of *Acynodon*, creating ambiguity between  
553 parsimony-based and Bayesian-based topologies. These results shorten the ghost lineage between  
554 *Hylaeochampsa* and *A. iberoccitanus* resulting from previous tip-dated Bayesian analyses of  
555 crocodylomorph taxa (Lee and Yates, 2018). The question of the monophyly of *Acynodon* is probably  
556 key to solve the relationships between hylaeochampsids and may bear some weight on the resolution  
557 of this clade inside Eusuchia (and early diverging eusuchian relationships overall). The morphological  
558 redescription and chronostrigraphic datum added herein are preliminary steps to increase the  
559 resolution at the base of Eusuchia and provide a better understanding of the palaeobiology and  
560 evolutionary history of this interesting clade of Mesozoic crocodylomorphs from the Tethyan domain.

561

## 562 **7. Conclusions**

563 A detailed description of specimen MCSNT 57031 herein referred to *Acynodon adriaticus*  
564 offers a new opportunity to evaluate the variation in the fossil eusuchians from Villaggio del Pescatore  
565 locality. The uppermost Cretaceous genus *Acynodon* is herein found monophyletic by the Bayesian  
566 analysis, with the Italian taxon representing an earlier diverging species from the lower-middle  
567 Campanian while the eponym taxon *Acynodon iberoccitanus* occupies a more recent  
568 chronostratigraphic range (middle-late Campanian). The Parsimony-based phylogenetic results,  
569 though, is in conflict with this interpretation, creating a paraphyletic *Acynodon*, probably also induced  
570 by the poorly phylogenetically sampled sister taxa (e.g. *Hylaeochampsa*), for which a redescription

571 and more complete phylogenetic scoring would be recommended (ideally, supplemented by new and  
572 more complete material). We highlight the need for a detailed and descriptive phylogenetic work  
573 focusing on key taxa at the base of Eusuchia, to resolve the phylogenetic relationships of these taxa  
574 (i.e. ‘hylaechampsids’) and resolve the taxonomy of *Acynodon*, with important possible  
575 repercussions on the palaeobiology of these remarkable peri-Tethyan crocodylomorphs, highlighted  
576 by the interesting asynchrony between histological and morphological maturity-related traits in its  
577 skeleton.

578

### 579 **Acknowledgments**

580 The authors thank all those involved in this research project on the Villaggio del Pescatore  
581 site: we hope scientific results will once again remark the uniqueness of this paleontological site and  
582 promote its protection and promotion by all institutional offices. The Soprintendenza Archeologia,  
583 Belle Arti e Paesaggio del Friuli Venezia Giulia facilitated the study of the vertebrate remains from  
584 the Villaggio del Pescatore (prot. 3289 dd. 22/02/2022 to F. Fanti). We wish to thank S. Bonomi and  
585 P. Ventura (SABAP) for their commitment to scientific research related to the Villaggio del Pescatore  
586 site. We thank P. Fasolato, F. Locci, D. Arbulla and the staff of the Museo Civico di Storia Naturale  
587 in Trieste for granting access to VdP material in their care. This work greatly benefited from the  
588 comments by the Editor E. Koutsoukos, A. Blanco and an anonymous reviewer. Discussions with L.  
589 Cantelli (UniBo) and L. Consorti (CNR-ISMAR) improved this manuscript. We are indebted with F.  
590 Bacchia and G. Bacchia (Zoic s.r.l.) for disclosing personal and historical information on the site. We  
591 also thank M. Sartori, F. Gamberini, and the Comune di Duino Aurisina. We acknowledge that images  
592 of specimens provided in this study are courtesy of Soprintendenza ABAP FVG -MiC (art. 108, co.3  
593 D. Lgs 42/2004 s.m.i). A.A.C. was supported through the European Research Council (ERC) starting  
594 grant under the European Union’s Horizon 2020 research and innovation program, grant agreement  
595 no. 947921, MAPAS at the Universidade de Vigo (Spain) and by a Juan de la Cierva-formación 2020

596 fellowship funded by FJC2020-044836-I/MCIN/AEI/10.13039/501100011033 by the European  
597 Union “NextGenerationEU”/PRTR.

598

- 600 Andrews, C.W., 1913. LVIII.—On the skull and part of the skeleton of a crocodile from the Middle  
601 Purbeck of Swanage, with a description of a new species (*Pholidosaurus laevis*), and a note  
602 on the skull of *Hylæochampsia*. *Annals and Magazine of Natural History* 11, 485–494.  
603 <https://doi.org/10.1080/00222931308693345>
- 604 Arbulla D., Cotza F., Cucchi F., Dalla Vecchia F.M., De Giusto A., Flora O., Masetti D., Palci A.,  
605 Pittau P., Pugliese N., Stenni B., Tarlao A., Tunis G. & Zini L., 2006. La successione  
606 Santoniano–Campaniana del Villaggio del Pescatore (Carso Triestino) nel quale sono stati  
607 rinvenuti i resti di dinosauro, in: Guida Alle Escursioni/Excursions Guide, Società  
608 Paleontologica Italiana. Presented at the Giornate di Paleontologia 2006, EUT Edizioni  
609 Università di Trieste, Trieste, pp. 20–27.
- 610 Attura, M., 1999. Aspetti paleontologici e geochimico-isotopici di una successione stratigrafica  
611 Santoniana-Campaniana del Villaggio del Pescatore (Ts). Università degli Studi di Trieste,  
612 Trieste.
- 613 Barrett, P.M., Butler, R.J., Mundil, R., Scheyer, T.M., Irmis, R.B., Sánchez-Villagra, M.R., 2014. A  
614 palaeoequatorial ornithischian and new constraints on early dinosaur diversification.  
615 *Proceedings of the Royal Society B: Biological Sciences* 281, 20141147.  
616 <https://doi.org/10.1098/rspb.2014.1147>
- 617 Bell, M.A., Lloyd, G.T., 2015. strap: an R package for plotting phylogenies against stratigraphy and  
618 assessing their stratigraphic congruence. *Palaeontology* 58, 379–389.  
619 <https://doi.org/10.1111/pala.12142>
- 620 Bennett, S.C., 1993. The ontogeny of *Pteranodon* and other pterosaurs. *Paleobiology* 19, 92–106.
- 621 Benton, M.J., Clark, J.M., 1988. Archosaur phylogeny and the relationships of the Crocodylia 295–  
622 338.
- 623 Blanco, A., 2021. Importance of the postcranial skeleton in eusuchian phylogeny: Reassessing the  
624 systematics of allodaposuchid crocodylians. *PLOS ONE* 16, e0251900.  
625 <https://doi.org/10.1371/journal.pone.0251900>
- 626 Blanco, A., Puértolas-Pascual, E., Marmi, J., Moncunill-Solé, B., Llácer, S., Rössner, G.E., 2020.  
627 Late Cretaceous (Maastrichtian) crocodyliforms from north-eastern Iberia: a first attempt to  
628 explain the crocodyliform diversity based on tooth qualitative traits. *Zoological Journal of*  
629 *the Linnean Society* 189, 584–617. <https://doi.org/10.1093/zoolinnean/zlz106>
- 630 Brinkmann, W., n.d. Die Krokodilier-Fauna aus der Unter-Kreide (Ober-Barremium) von Una  
631 (Provinz Cuenca, Spanien). Herausgegeben von geowissenschaftlichen Instituten der Freien  
632 und der Technischen Universität Berlin und der Technischen Fachhochschule Berlin.
- 633 Brochu, C.A., 2012. Phylogenetic relationships of Palaeogene ziphodont eusuchians and the status  
634 of *Pristichampsus* Gervais, 1853. *Earth and Environmental Science Transactions of The*  
635 *Royal Society of Edinburgh* 103, 521–550. <https://doi.org/10.1017/S1755691013000200>
- 636 Brochu, C.A., 2011. Phylogenetic relationships of *Necrosuchus ionensis* Simpson, 1937 and the  
637 early history of caimanines. *Zoological Journal of the Linnean Society* 163, S228–S256.  
638 <https://doi.org/10.1111/j.1096-3642.2011.00716.x>
- 639 Brochu, C.A., 2010. A new alligatorid from the lower Eocene Green River Formation of Wyoming  
640 and the origin of caimans. *Journal of Vertebrate Paleontology* 30, 1109–1126.  
641 <https://doi.org/10.1080/02724634.2010.483569>
- 642 Brochu, C.A., 2003. Phylogenetic Approaches Toward Crocodylian History. *Annu. Rev. Earth*  
643 *Planet. Sci.* 31, 357–397. <https://doi.org/10.1146/annurev.earth.31.100901.141308>
- 644 Brochu, C.A., 2001. Crocodylian snouts in space and time: phylogenetic approaches toward  
645 adaptive radiation. *American Zoologist* 41, 564–585. <https://doi.org/10.1093/icb/41.3.564>
- 646 Brochu, C.A., 1999. Phylogenetics, Taxonomy, and Historical Biogeography of Alligatoroidea.  
647 *Journal of Vertebrate Paleontology* 19, 9–100.  
648 <https://doi.org/10.1080/02724634.1999.10011201>

- 649 Brochu, C.A., 1996. Closure of neurocentral sutures during crocodylian ontogeny: Implications for  
650 maturity assessment in fossil archosaurs. *Journal of Vertebrate Paleontology* 16, 49–62.  
651 <https://doi.org/10.1080/02724634.1996.10011283>
- 652 Brochu, C.A., Parris, D.C., Grandstaff, B.S., Denton, R.K., Gallagher, W.B., 2012. A new species  
653 of *Borealosuchus* (Crocodyliformes, Eusuchia) from the Late Cretaceous–early Paleogene  
654 of New Jersey. *Journal of Vertebrate Paleontology* 32, 105–116. <https://doi.org/10.1080/02724634.2012.633585>
- 655 Brochu, C.A., Storrs, G.W., 2012. A giant crocodile from the Plio-Pleistocene of Kenya, the  
656 phylogenetic relationships of Neogene African crocodylines, and the antiquity of  
657 *Crocodylus* in Africa. *Journal of Vertebrate Paleontology* 32, 587–602.  
658 <https://doi.org/10.1080/02724634.2012.652324>
- 659 Buscalioni, A.D., Ortega, F., Vasse, D., 1997. New crocodiles (Eusuchia: Alligatoroidea) from the  
660 Upper Cretaceous of southern Europe. *Comptes Rendus de l'Académie des Sciences - Series*  
661 *IIA - Earth and Planetary Science* 325, 525–530. [https://doi.org/10.1016/S1251-](https://doi.org/10.1016/S1251-8050(97)89872-2)  
662 [8050\(97\)89872-2](https://doi.org/10.1016/S1251-8050(97)89872-2)
- 663 Carr, T.D., 1999. Craniofacial ontogeny in tyrannosauridae (Dinosauria, Coelurosauria). *Journal of*  
664 *vertebrate Paleontology* 19, 497–520.
- 665 Cerda, I.A., Desojo, J.B., 2011. Dermal armour histology of aetosaurs (Archosauria: Pseudosuchia),  
666 from the Upper Triassic of Argentina and Brazil. *Lethaia* 44, 417–428.  
667 <https://doi.org/10.1111/j.1502-3931.2010.00252.x>
- 668 Chiappe, L.M., Göhlich, U.B., 2010. Anatomy of *Juravenator starki* (Theropoda: Coelurosauria)  
669 from the late Jurassic of Germany. *Neues Jahrbuch fuer Geologie und Palaeontologie.*  
670 *Abhandlungen* 258, 257–296.
- 671 Chiarenza, A.A., Fabbri, M., Consorti, L., Muscioni, M., Evans, D.C., Cantalapiedra, J.L., Fanti, F.,  
672 2021. An Italian dinosaur Lagerstätte reveals the tempo and mode of hadrosauriform body  
673 size evolution. *Scientific Reports* 11, 23295. <https://doi.org/10.1038/s41598-021-02490-x>
- 674 Chiarenza, A.A., Fiorillo, A.R., Tykoski, R.S., McCarthy, P.J., Flaig, P.P., Contreras, D.L., 2020.  
675 The first juvenile dromaeosaurid (Dinosauria: Theropoda) from Arctic Alaska. *PLOS ONE*  
676 15, e0235078. <https://doi.org/10.1371/journal.pone.0235078>
- 677 Consorti, L., Arbutta, D., Bonini, L., Fabbri, S., Fanti, F., Franceschi, M., Frijia, G., Pini, G.A.,  
678 2021. The Mesozoic palaeoenvironmental richness of the Trieste Karst. *GFT&M.*  
679 <https://doi.org/10.3301/GFT.2021.06>
- 680 Dalla Vecchia, F.M., 2009. *Tethyshadros insularis*, a new hadrosauroid dinosaur (Ornithischia)  
681 from the Upper Cretaceous of Italy. *Journal of Vertebrate Paleontology* 29, 1100–1116.  
682 <https://doi.org/10.1671/039.029.0428>
- 683 Dalla Vecchia, F.M., 2008. I dinosauri del Villaggio del Pescatore (Trieste): qualche aggiornamento  
684 21.
- 685 Dalla Vecchia, F.M., 1999. Relazione scientifica finale, scavo paleontologico del Villaggio del  
686 Pescatore 1998-1999 & elencazione, identificazione e determinazione preliminare dei  
687 reperti.
- 688 de Ricqlès, A.J., Padian, K., Horner, J.R., 2003. On the bone histology of some Triassic  
689 pseudosuchian archosaurs and related taxa. *Annales de Paléontologie* 89, 67–101.  
690 [https://doi.org/10.1016/S0753-3969\(03\)00005-3](https://doi.org/10.1016/S0753-3969(03)00005-3)
- 691 Deeming, D.C., Ferguson, M.W.J., 1990. Morphometric analysis of embryonic development in  
692 *Alligator mississippiensis*, *Crocodylus johnstoni* and *Crocodylus porosus*. *Journal of*  
693 *Zoology* 221, 419–439. <https://doi.org/10.1111/j.1469-7998.1990.tb04011.x>
- 694 Delfino, M., Buffetaut, E., 2006. A preliminary description of the crocodylian remains from the  
695 Late Cretaceous of Villaggio del Pescatore (northeastern Italy).
- 696 Delfino, Massimo, Martin, J.E., Buffetaut, E., 2008a. A new species of *Acynodon* (Crocodylia)  
697 from the upper cretaceous (Santonian–Campanian) of Villaggio del Pescatore, Italy.  
698 *Palaeontology* 51, 1091–1106. <https://doi.org/10.1111/j.1475-4983.2008.00800.x>

- 699 Delfino, M., Martin, J.E., Buffetaut, E., 2008b. I coccodrilli del Villaggio del Pescatore: una  
700 panoramica generale. *Atti del Museo Civico di Storia Naturale di Trieste* 53, 277–284.
- 701 Dodson, P., 1975. Taxonomic Implications of Relative Growth in Lambeosaurine Hadrosaurs.  
702 *Systematic Zoology* 24, 37–54. <https://doi.org/10.2307/2412696>
- 703 Erickson, G.M., Brochu, C.A., 1999. How the ‘terror crocodile’ grew so big. *Nature* 398, 205–206.  
704 <https://doi.org/10.1038/18343>
- 705 Frijia, G., Parente, M., Di Lucia, M., Mutti, M., 2015. Carbon and strontium isotope stratigraphy of  
706 the Upper Cretaceous (Cenomanian-Campanian) shallow-water carbonates of southern Italy:  
707 Chronostratigraphic calibration of larger foraminifera biostratigraphy. *Cretaceous Research*  
708 53, 110–139. <https://doi.org/10.1016/j.cretres.2014.11.002>
- 709 Goloboff, P.A., Farris, J.S., Nixon, K.C., 2008. TNT, a free program for phylogenetic analysis.  
710 *Cladistics* 24, 774–786. <https://doi.org/10.1111/j.1096-0031.2008.00217.x>
- 711 Gregorovičová, M., Kvasilová, A., Sedmera, D., 2018. Ossification Pattern in Forelimbs of the  
712 Siamese Crocodile (*Crocodylus siamensis*): Similarity in Ontogeny of Carpus Among  
713 Crocodylian Species. *The Anatomical Record* 301, 1159–1168.  
714 <https://doi.org/10.1002/ar.23792>
- 715 Griffin, C.T., Stocker, M.R., Colleary, C., Stefanic, C.M., Lessner, E.J., Riegler, M., Formoso, K.,  
716 Koeller, K., Nesbitt, S.J., 2021. Assessing ontogenetic maturity in extinct saurian reptiles.  
717 *Biological Reviews* 96, 470–525. <https://doi.org/10.1111/brv.12666>
- 718 Hone, D.W.E., Farke, A.A., Wedel, M.J., 2016. Ontogeny and the fossil record: what, if anything, is  
719 an adult dinosaur? *Biology Letters* 12, 20150947. <https://doi.org/10.1098/rsbl.2015.0947>
- 720 Huchzermeyer, F.W., Groenewald, H.B., Myburgh, J.G., Steyl, J.C.A., Crole, M.R., 2013.  
721 Osteoarthropathy of unknown aetiology in the long bones of farmed and wild Nile  
722 crocodiles (*Crocodylus niloticus*). *Journal of the South African Veterinary Association* 84,  
723 1–5.
- 724 Jones, L.A., Gearty, W., Allen, B.J., Eichenseer, K., Dean, C.D., Galván, S., Kouvari, M., Godoy,  
725 P.L., Nicholl, C.S.C., Buffan, L., Dillon, E.M., Flannery-Sutherland, J.T., Chiarenza, A.A.,  
726 2023. palaeoverse: A community-driven R package to support palaeobiological analysis.  
727 *Methods in Ecology and Evolution* n/a. <https://doi.org/10.1111/2041-210X.14099>
- 728 Jouve, S., Sarigül, V., Steyer, J.-S., Sen, S., 2019. The first crocodylomorph from the Mesozoic of  
729 Turkey (Barremian of Zonguldak) and the dispersal of the eusuchians during the Cretaceous.  
730 *Journal of Systematic Palaeontology* 17, 111–128.  
731 <https://doi.org/10.1080/14772019.2017.1393469>
- 732 Jurkovšek, B., Biolchi, S., Furlani, S., Kolar-Jurkovšek, T., Zini, L., Jež, J., Tunis, G., Bavec, M.,  
733 Cucchi, F., 2016. Geology of the Classical Karst Region (SW Slovenia–NE Italy). *Journal*  
734 *of Maps* 12, 352–362. <https://doi.org/10.1080/17445647.2016.1215941>
- 735 Kramer, G., Medem, F., 1955. Über wachstumsbedingte Proportionsänderungen bei Krokodilen.  
736 *Zoologische Jahrbücher* 66, 62–74.
- 737 Lee, M.S.Y., Cau, A., Naish, D., Dyke, G.J., 2014. Morphological Clocks in Paleontology, and a  
738 Mid-Cretaceous Origin of Crown Aves. *Systematic Biology* 63, 442–449.  
739 <https://doi.org/10.1093/sysbio/syt110>
- 740 Lima, F., Santos, A., Vieira, L., Coutinho, M., 2011. Ossification sequence of skull and hyoid in  
741 embryos of Caiman yacare (Crocodylia, Alligatoridae). *Iheringia. Série Zoologia* 101, 161–  
742 172. <https://doi.org/10.1590/S0073-47212011000200003>
- 743 Mannion, P.D., Chiarenza, A.A., Godoy, P.L., Cheah, Y.N., 2019. Spatiotemporal sampling  
744 patterns in the 230 million year fossil record of terrestrial crocodylomorphs and their impact  
745 on diversity. *Palaeontology* 62, 615–637. <https://doi.org/10.1111/pala.12419>
- 746 Martin, J.E., 2007. New Material of the Late Cretaceous Globidontan *Acynodon iberoccitanus*  
747 (Crocodylia) from Southern France. *Journal of Vertebrate Paleontology* 27, 362–372.
- 748 Martin, J.E., Delfino, M., Garcia, G., Godefroit, P., Berton, S., Valentin, X., 2016. New specimens  
749 of *Allodaposuchus precedens* from France: intraspecific variability and the diversity of

- 750 European Late Cretaceous eusuchians. *Zoological Journal of the Linnean Society* 176, 607–  
751 631. <https://doi.org/10.1111/zoj.12331>
- 752 Martin, J.E., Smith, T., de Lapparent de Broin, F., Escuillié, F., Delfino, M., 2014. Late Palaeocene  
753 eusuchian remains from Mont de Berru, France, and the origin of the alligatoroid  
754 *Diplocynodon*. *Zoological Journal of the Linnean Society* 172, 867–891.  
755 <https://doi.org/10.1111/zoj.12195>
- 756 Martin, J.E., Smith, T., Salaviale, C., Adrien, J., Delfino, M., 2020. Virtual reconstruction of the  
757 skull of *Bernissartia fagesii* and current understanding of the neosuchian–eusuchian  
758 transition. *Journal of Systematic Palaeontology* 18, 1079–1101.  
759 <https://doi.org/10.1080/14772019.2020.1731722>
- 760 Motani, R., Jiang, D.-Y., Tintori, A., Rieppel, O., Chen, G.-B., You, H., 2015. First evidence of  
761 centralia in Ichthyopterygia reiterating bias from pedomorphic characters on marine reptile  
762 phylogenetic reconstruction. *Journal of Vertebrate Paleontology* 35, e948547.  
763 <https://doi.org/10.1080/02724634.2014.948547>
- 764 Müller, G.B., Alberch, P., 1990. Ontogeny of the limb skeleton in *Alligator mississippiensis*:  
765 Developmental invariance and change in the evolution of archosaur limbs. *Journal of*  
766 *Morphology* 203, 151–164. <https://doi.org/10.1002/jmor.1052030204>
- 767 Narváez, I., Brochu, C.A., Escaso, F., Pérez-García, A., Ortega, F., 2016. New Spanish Late  
768 Cretaceous eusuchian reveals the synchronic and sympatric presence of two  
769 allodaposuchids. *Cretaceous Research* 65, 112–125.  
770 <https://doi.org/10.1016/j.cretres.2016.04.018>
- 771 Nesbitt, S.J., 2011. The early evolution of archosaurs : relationships and the origin of major clades.  
772 (*Bulletin of the American Museum of Natural History*, no. 352).
- 773 Palci, A., 2003. Ricostruzione Paleoambientale del Sito Fossilifero Senoniano del Villaggio del  
774 Pescatore (Trieste) (Tesi di Laurea In Paleontologia). Università degli Studi di Trieste,  
775 Trieste.
- 776 Parker, W.G., Stocker, M.R., Irmis, R.B., 2008. A New Desmotosuchine Aetosaur (Archosauria:  
777 Suchia) from the Upper Triassic Tecovas Formation (Dockum Group) of Texas. *Journal of*  
778 *Vertebrate Paleontology* 28, 692–701.
- 779 Ponce, D., Cerda, I., Desojo, J., Nesbitt, S., 2017. The osteoderm microstructure in doswelliids and  
780 proterochampsids and its implications for palaeobiology of stem archosaurs. *APP* 62.  
781 <https://doi.org/10.4202/app.00381.2017>
- 782 Puértolas-Pascual, E., Young, M.T., Brochu, C.A., 2020. Introducing the First European  
783 Symposium on the Evolution of Crocodylomorpha. *Zoological Journal of the Linnean*  
784 *Society* 189, 419–427. <https://doi.org/10.1093/zoolinnea/zlaa012>
- 785 Rambaut, A., Drummond, A.J., Xie, D., Baele, G., Suchard, M.A., 2018. Posterior Summarization  
786 in Bayesian Phylogenetics Using Tracer 1.7. *Systematic Biology* 67, 901–904.  
787 <https://doi.org/10.1093/sysbio/syy032>
- 788 Raven, T.J., Maidment, S.C.R., 2018. The systematic position of the enigmatic thyreophoran  
789 dinosaur *Paranthodon africanus*, and the use of basal exemplifiers in phylogenetic analysis.  
790 *PeerJ* 6, e4529. <https://doi.org/10.7717/peerj.4529>
- 791 Rieppel, O., 1989. The Hind Limb of *Macrocnemus bassanii* (Nopcsa) (Reptilia, Diapsida):  
792 Development and Functional Anatomy. *Journal of Vertebrate Paleontology* 9, 373–387.
- 793 Rio, J.P., Mannion, P.D., 2021. Phylogenetic analysis of a new morphological dataset elucidates the  
794 evolutionary history of Crocodylia and resolves the long-standing gharial problem. *PeerJ* 9,  
795 e12094. <https://doi.org/10.7717/peerj.12094>
- 796 Ristevski, J., Yates, A.M., Price, G.J., Molnar, R.E., Weisbecker, V., Salisbury, S.W., 2020.  
797 Australia’s prehistoric ‘swamp king’: revision of the Plio-Pleistocene crocodylian genus  
798 *Pallimnarchus* de Vis, 1886. *PeerJ* 8, e10466. <https://doi.org/10.7717/peerj.10466>

- 799 Sampson, S.D., Ryan, M.J., Tanke, D.H., 1997. Craniofacial ontogeny in centrosaurine dinosaurs  
800 (Ornithischia: Ceratopsidae): taxonomic and behavioral implications. *Zoological Journal of*  
801 *the Linnean Society* 121, 293–337.
- 802 Scheyer, T.M., Desojo, J., 2011. Palaeohistology and external microanatomy of rauisuchian  
803 osteoderms (Archosauria: Pseudosuchia). *Palaeontology* 54, 1289–1302.  
804 <https://doi.org/10.1111/j.1475-4983.2011.01098.x>
- 805 Scheyer, T.M., Sander, P.M., 2009. Bone microstructures and mode of skeletogenesis in osteoderms  
806 of three pareiasaur taxa from the Permian of South Africa. *Journal of Evolutionary Biology*  
807 22, 1153–1162. <https://doi.org/10.1111/j.1420-9101.2009.01732.x>
- 808 Stubbs, T.L., Pierce, S.E., Elsler, A., Anderson, P.S.L., Rayfield, E.J., Benton, M.J., 2021.  
809 Ecological opportunity and the rise and fall of crocodylomorph evolutionary innovation.  
810 *Proceedings of the Royal Society B: Biological Sciences* 288, 20210069.  
811 <https://doi.org/10.1098/rspb.2021.0069>
- 812 Taborda J. R. A., Cerda I. A., Desojo J. B., 2013. Growth curve of *Aetosauroides scagliai*  
813 *Casamiquela 1960* (Pseudosuchia: Aetosauria) inferred from osteoderm histology.  
814 *Geological Society, London, Special Publications* 379, 413–423.  
815 <https://doi.org/10.1144/SP379.19>
- 816 Tarlao, A., Tentor, M., Tunis, G., Venturini, S., 1995. Stop 4: Villaggio del Pescatore. *Atti Museo*  
817 *Geologico Paleontologico Monfalcone* 135–142.
- 818 Tarlao A., Tentor M., Tunis G., Venturini S., 1993. Evidenze di una fase tettonica nel Senoniano  
819 inferiore dell'area del Villaggio del Pescatore (Trieste). *Gortania Atti Museo Friulano Storia*  
820 *Naturale* 23–24.
- 821 Tumarkin-Deratzian, A.R., Vann, D.R., Dodson, P., 2006. Bone surface texture as an ontogenetic  
822 indicator in long bones of the Canada goose *Branta canadensis* (Anseriformes: Anatidae).  
823 *Zoological Journal of the Linnean Society* 148, 133–168. [https://doi.org/10.1111/j.1096-](https://doi.org/10.1111/j.1096-3642.2006.00232.x)  
824 [3642.2006.00232.x](https://doi.org/10.1111/j.1096-3642.2006.00232.x)
- 825 Vieira, L.G., Lima, F.C., Mendonça, S.H.S.T., Menezes, L.T., Hirano, L.Q.L., Santos, A.L.Q.,  
826 2018. Ontogeny of the Postcranial Axial Skeleton of *Melanosuchus niger* (Crocodylia,  
827 Alligatoridae). *The Anatomical Record* 301, 607–623. <https://doi.org/10.1002/ar.23722>
- 828 von Baczko, M.B., Desojo, J.B., Ponce, D., 2019. Postcranial anatomy and osteoderm histology of  
829 *Riojasuchus tenuisiceps* and a phylogenetic update on Ornithosuchidae (Archosauria,  
830 Pseudosuchia). *Journal of Vertebrate Paleontology* 39, e1693396.  
831 <https://doi.org/10.1080/02724634.2019.1693396>
- 832 Witzmann, F., 2009. Comparative histology of sculptured dermal bones in basal tetrapods, and the  
833 implications for the soft tissue dermis.
- 834 Witzmann, F., Soler-Gijón, R., 2010. The bone histology of osteoderms in temnospondyl  
835 amphibians and in the chroniosuchian *Bystrowiella*. *Acta Zoologica* 91, 96–114.  
836 <https://doi.org/10.1111/j.1463-6395.2008.00385.x>
- 837 Woodward Ballard, H., Horner, J., Farlow, J., 2011. Osteohistological Evidence for Determinate  
838 Growth in the American Alligator. *Journal of Herpetology* 45, 339–342.  
839 <https://doi.org/10.1670/10-274.1>
- 840 Woodward, H.N., Horner, J.R., Farlow, J.O., 2014. Quantification of intraskeletal histovariability in  
841 *Alligator mississippiensis* and implications for vertebrate osteohistology. *PeerJ* 2, e422.  
842 <https://doi.org/10.7717/peerj.422>  
843

844 **Figure captions**



845 **Figure 1.** Specimen of *Acynodon adriaticus* MCSNT 57031. Laminite slab with the specimen embedded in  
846 matrix (A) and anatomical elements highlighted in B. Abbreviations: c: cervical vertebrae, icl: interclavicle,  
847 lhu: left humerus, lmr: left mandibular ramus, lr: left radius, lu: left ulna, ost: osteoderms, rb: ribs, rca:  
848 radiale carpal, rco: right coracoid, rhu: right humerus, rmc: right metacarpals, rmr: right mandibular ramus,  
849 rmx: right maxilla, rph: right phalanges, rr: right radius, ru: right ulna. Scale bar: 5 cm.

850

851 **Figure 2.** Isolated or fragmentary specimens referred to *Acynodon adriaticus*. A: MCSNT21.S239-1.0.22  
852 (57248a), B: MCSNT 57245, C: MCSNT21.S239-1.0.22 (57248b). Scale bar: 5 cm.

853 **Figure 3.** Geographic and geological setting of the Villaggio del Pescatore quarry. Geographic location of  
854 the site (A); orthophotographic view of the quarry obtained with UAV and photogrammetric processing (B),  
855 simplified geological map of the site (C) and location of the specimen in the quarry superimposed to GIS-  
856 based orthophoto (D). S, slumped rhythmites, L, laminites. Core S3 is the reference core for biostratigraphic  
857 analyses (*see* Chiarenza et al., 2021).

858 **Figure 4.** Skull of MCSNT 57031 (A), with anatomical labels in B. Abbreviations: cs: condylar surface, lrp:  
859 left retroarticular process, or: ornamentations, rd: right dentary, rmx: right maxilla, rrp: right retroarticular  
860 process. Scale bar: 5 cm.

861 **Figure 5.** Cranial outlines in ventral views of specimens referred to *Acynodon adriaticus*, with MCSNT  
862 57031 (A) and the holotype MCSNT 57248 (B). Scale bar: 5 cm.

863 **Figure 6.** Close-up of the dentary of MCSNT 57031 in cranioventral view. Scale bar: 1 cm.

864 **Figure 7.** Cervical series of MCSNT 57031 in lateral view (A) with anatomical labels and outlines  
865 highlighted in B. Abbreviations: c: cervical, cr: cervical ribs. Scale bar: 5 cm.

866 **Figure 8.** Ribs of MCSNT 57031 in lateral view with gastralia highlighted in different colours (red) than  
867 dorsal ribs (blue). Abbreviations: rb: ribs. Scale bar: 5 cm.

868 **Figure 9.** Pectoral girdle elements of MCSNT 57031 in lateral view. Abbreviations: icl: interclavicle, lco:  
869 left coracoid, lsc: left scapula, rco: right coracoid, rsc: right scapula. Scale bar: 5 cm.

870 **Figure 10.** Right forelimb elements of MCSNT 57031. Arrows indicate restoration in the zeugopodium.  
871 Abbreviations: dca: distale carpal, dpc: deltopectoral crest, icl: interclavicle, mc: metacarpal, pca: pisiform  
872 carpal, ph: phalanges, rca: radiale carpal, rco: right coracoid, rhu: right humerus, rr: right radius, rsc: right  
873 scapula, ru: right ulna, uca: ulnare carpal. Scale bar: 5 cm

874 **Figure 11.** Details of right forelimb elements of MCSNT 57031. Arrows indicate osteoporotic surfaces.  
875 Abbreviations: dpc: deltopectoral crest, rhu: right humerus, rr: right radius, ru: right ulna. Scale bar: 5 cm.

876 **Figure 12.** Details of right autopodium elements of MCSNT 57031. Arrows indicate osteoporotic articular  
877 surfaces. Abbreviations: dca: distale carpal, mc: metacarpal, pca: pisiform carpal, ph: phalanges, rca: radiale  
878 carpal, uca: ulnare carpal, ?cca, possible fragments of the central carpal (centrale). Scale bar: 1 cm.

879 **Figure 13.** Left forelimb elements of MCSNT 57031 (A) with anatomical labels reported in B.  
880 Abbreviations: lhu: left humerus, lr: left radius, lu: left ulna, mc: metacarpals, ph: phalanges, rca: radiale  
881 carpal, uca: ulnare carpal. Scale bar: 5 cm.

882 **Figure 14.** Osteodermal series of MCSNT 57031 sketched and in different light direction (A) and  
883 morphological outlines of the best-preserved ones in B. Black triangle points to possible ventrally exposed  
884 osteoderms (*see* section 4.2). Arrows points to the direction towards the cranium of the specimen. Scale bars:  
885 5 cm.

886 **Figure 15.** Histological thin sections under polarised light of MCSNT 57031 6th dorsal rib. A, overall rib  
887 histological section; B, detail of secondary osteons, C, lines of arrested growth (LAGs) and annuli in the  
888 outer cortex of the rib section; D, overview of the osteoderm thin section; E, close up of the outer cortex of  
889 the osteoderm. Scale bars in: B, 250 nm; C, 500 nm; E, 200 nm. Abbreviations: An: annuli; cb: cancellous  
890 bone; ec: erosional cavity; hs: haversian system; pv: primary vascularization. Red arrows indicate LAGs.

891 **Figure 16.** Phylogenetic position of *Acynodon adriaticus*. Results of Maximum Parsimony with strict  
892 consensus (A) and majority rule (B) trees. Time calibrated Bayesian tree focused on the base of Eusuchia  
893 (C). Yellow box is used to highlight the position of the genus *Acynodon*. Specimens referred to *Acynodon*  
894 *adriaticus* highlighted in red. Abbreviation in the chronological y-axis 'Ma' refers to Mega annum (million

895 years). Numbers in A indicate Bremer support (Decay index) while bootstrap support values are reported for  
896 the Majority rule tree in B.

897 **Figure 17.** Skeletal reconstruction of MCSNT 57031 in A with size comparison between the latter specimen  
898 in ventral view and the holotype (more complete in dorsal view) in B.

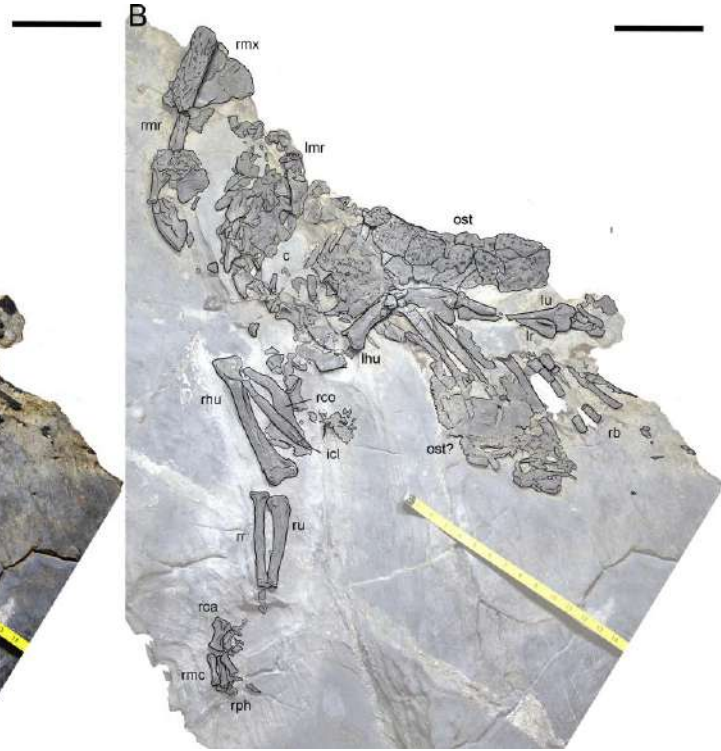
899 **Table 1.** List of crocodylian remains found at the Villaggio del Pescatore site. VP, Villaggio del Pescatore,  
900 progressive numbers referring to limestone blocks quarried in order to collect vertebrate remains.

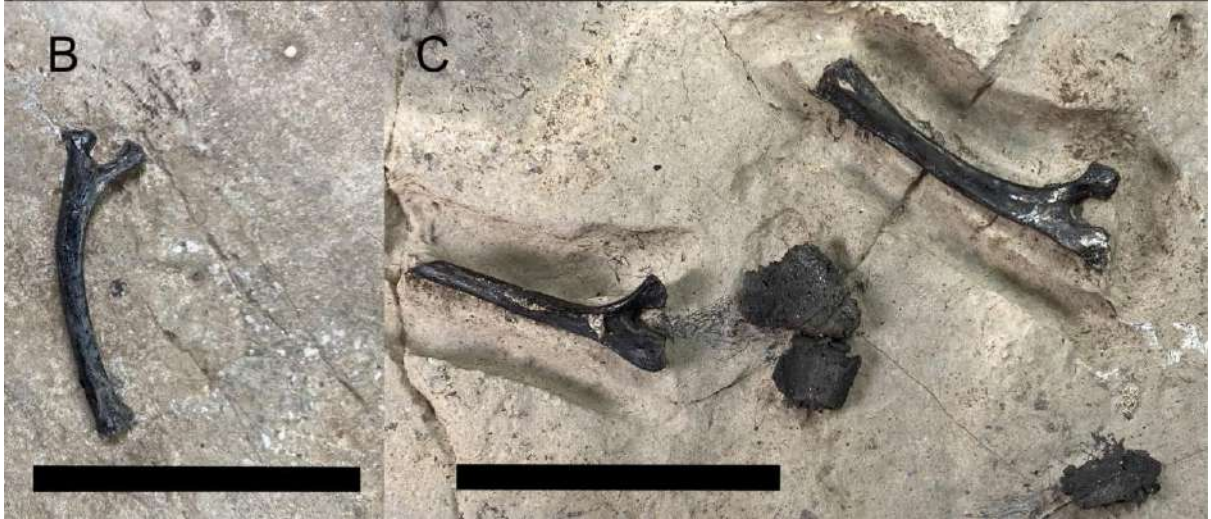
901

SPECIMENT INVENTORY	SPECIMEN DESCRIPTION	QUARRY INFORMATI ON
<i>Acynodon adriaticus</i>		
MCNST 57248	Holotype, Delfino et al., 2008	Collected near VP12, about 55 cm above VP1 in 1998-1999
MCNST 57032	Paratype, Delfino et al., 2008	Collected in the proximity of the holotype in 1996-1997
<b>New specimens assigned to <i>Acynodon adriaticus</i> and discussed in this study</b>		
MCSNT 57031	ventrally exposed, articulated, sub-complete specimen	Collected in VP4 in the same horizon as VP2 in 1996- 1997
MCSNT 57245	an isolated, well preserved robust crocodylian rib laying on the flat surface of a larger matrix slab with other unidentified bone fragments. The tuberculum is shorter than the capitulum and	Collected from Slab 38 in 1998-1999

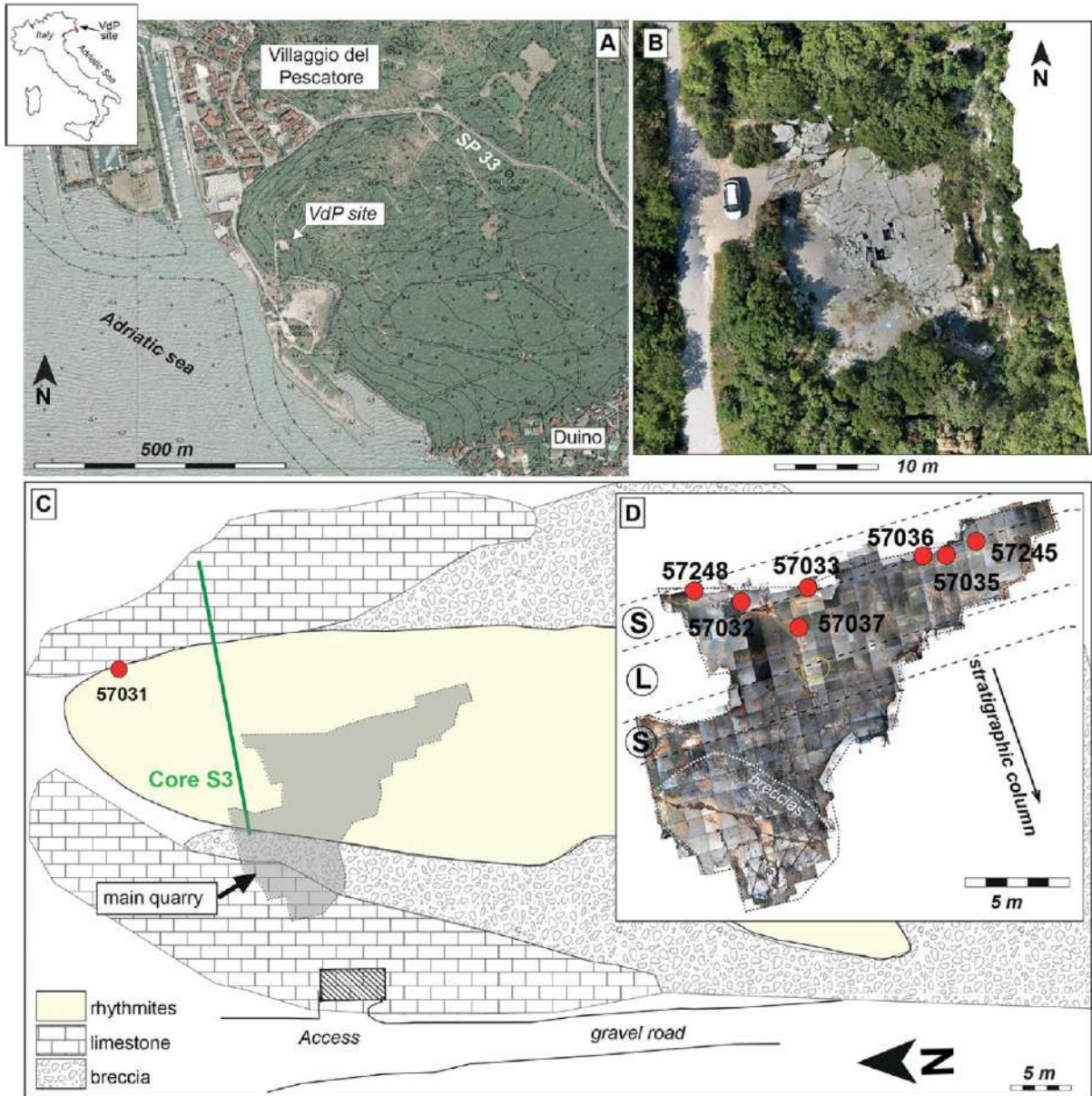
	apparently has a larger articular surface. The rib progressively thickens distally and has a wide costal cartilage articular surface	
MCSNT 21.S239-1.0.22 (57248a)	six well preserved osteoderms, three of them in partial overlap. The larger ones, measured at their longer axis, are 22,8 mm, 24,5 mm and 27 mm long respectively. These osteoderms show two low keels, one straight and the other concave and larger, comparable to the condition described in the paratype by Delfino et al., 2008	Collected near the holotype in 1998-1999
MCSNT 21.S239-1.0.22 (57248b)	three small osteoderms and two robust ribs in association, both showing shorter and stouter tubercula than capitula, with wider articular surfaces. The shorter rib measures 46,7 mm in length and lacks its distalmost portion; the longer one measures 57,2 mm, appears to be complete and gradually thickens at its distal end, revealing a large costal cartilage articular surface.	Collected near the holotype in 1998-1999
<b>Specimens assigned to Crocodylomorpha indet.</b>		
MCSNT 57033	a ~4 cm long unidentified small reptile bone, possibly a rib, exposing its sagittal section on the surface of a small laminite fragment.	Collected in the proximity of the holotype in 1998-1999
MCSNT 57035	a ~5 cm long bone element exposed on a calcareous slab with an ornamented surface, here identified as a ventrally exposed crocodylian mandibular symphysis	Collected from Slab 41 in 1998-1999
MCSNT 57036	a ~2 cm anteroposteriorly long vertebra, possibly a fragmented cervical, three-dimensionally prepared out of the matrix	Collected from Slab 41 in 1998-1999

MCSNT 57037	an almost unrecognizable smooth bone fragment hardly visible on a small matrix slab associated with other indeterminate vertebrate fossil material, previously tentatively identified as a fragmented ventral osteodermal surface	Collected from Slab 15 in 1996-1997 and 1998-1999
-------------	---	---





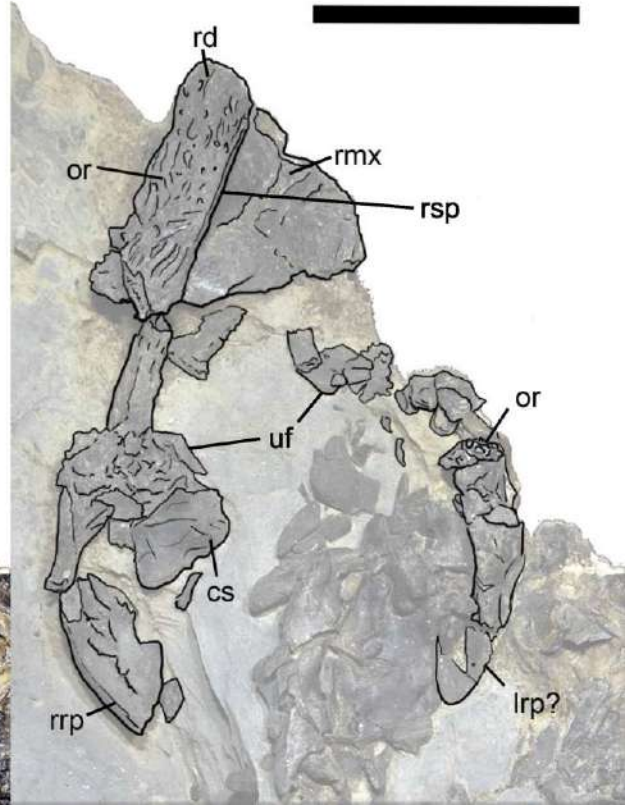




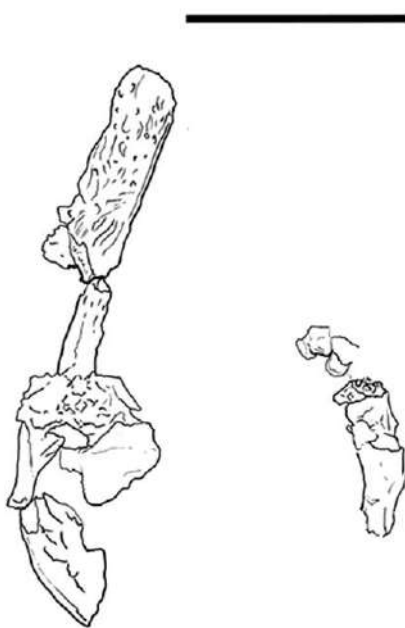
A



B



A

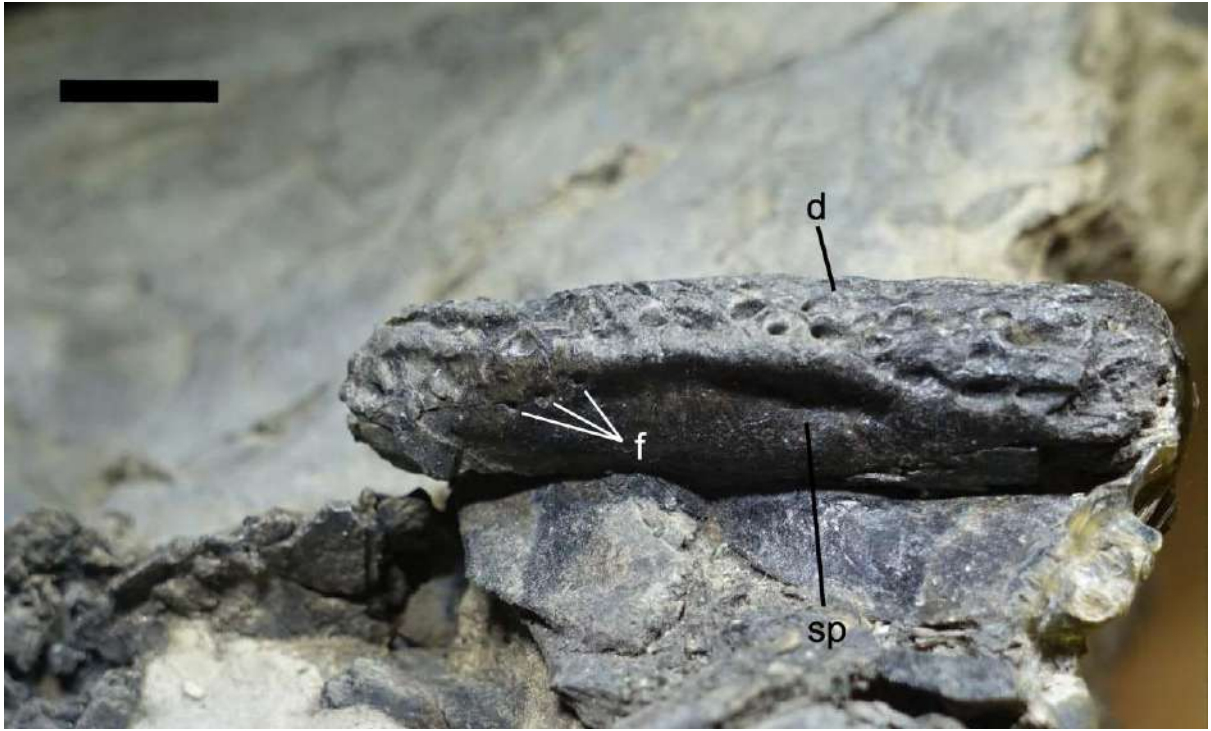


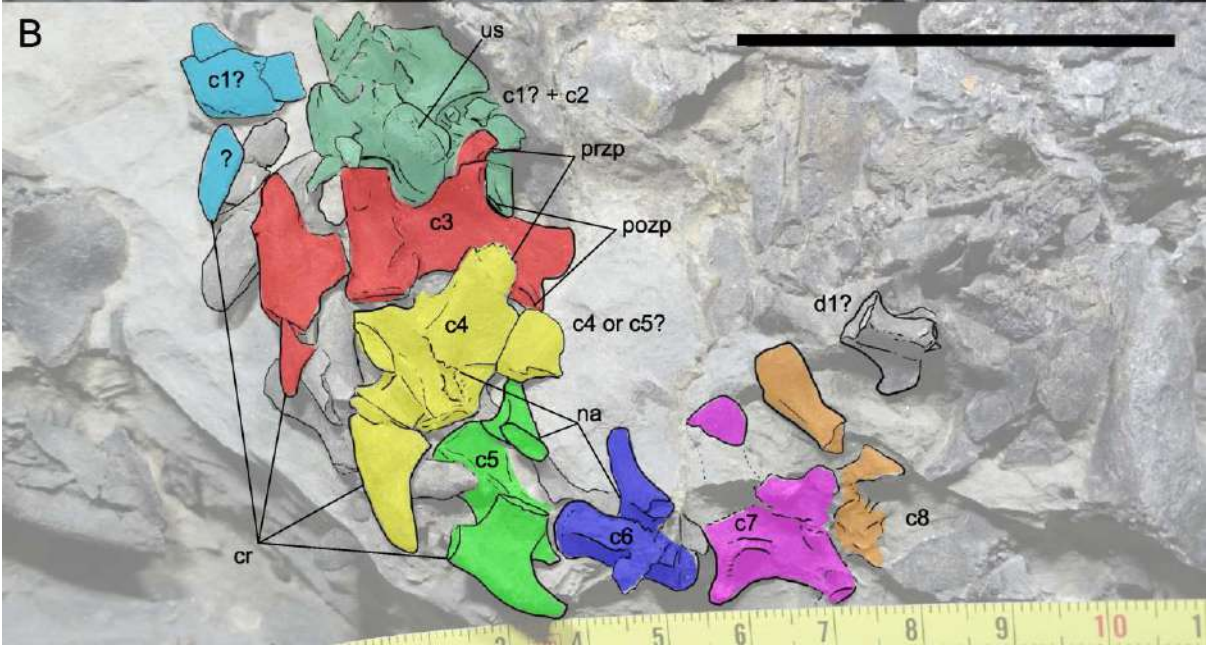
MCSNT 57031

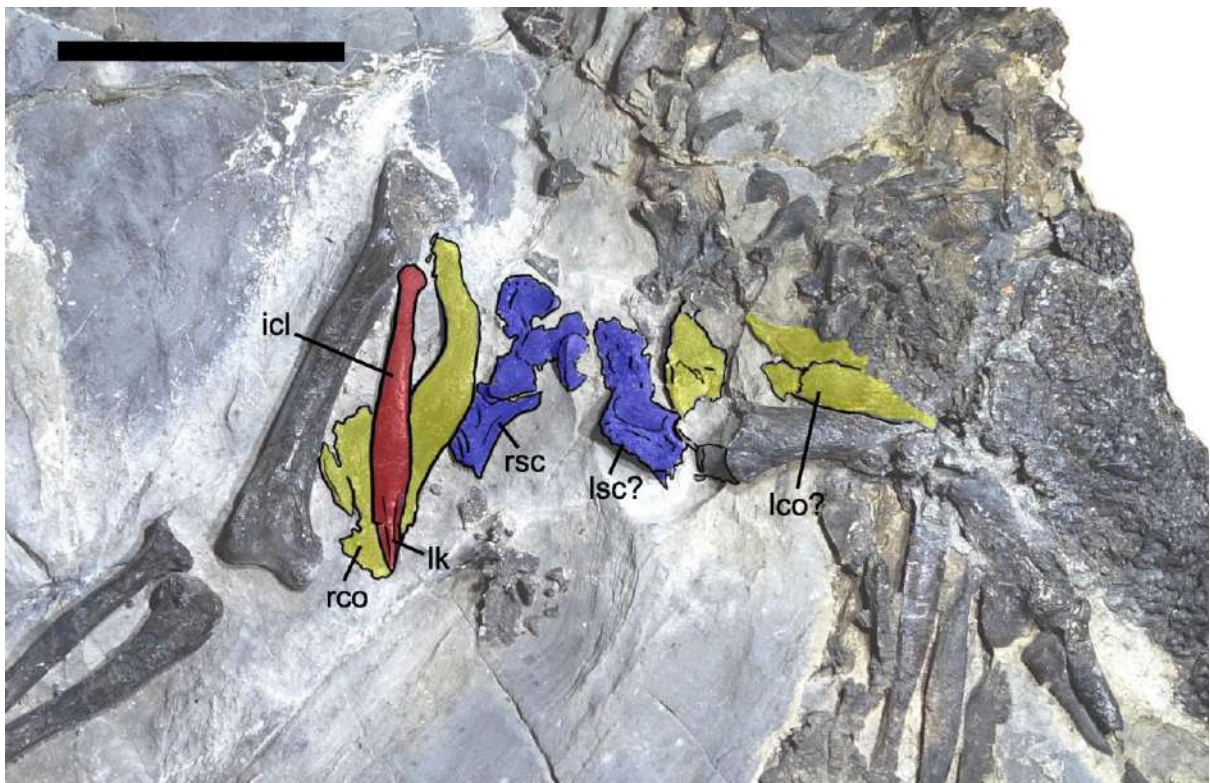
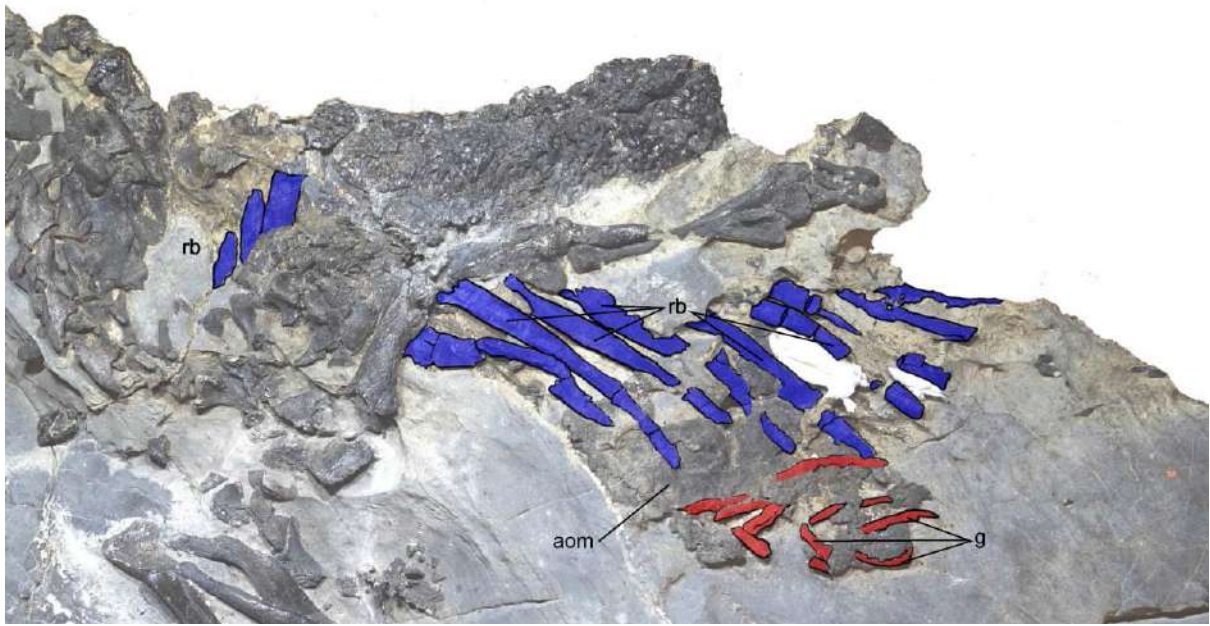
B

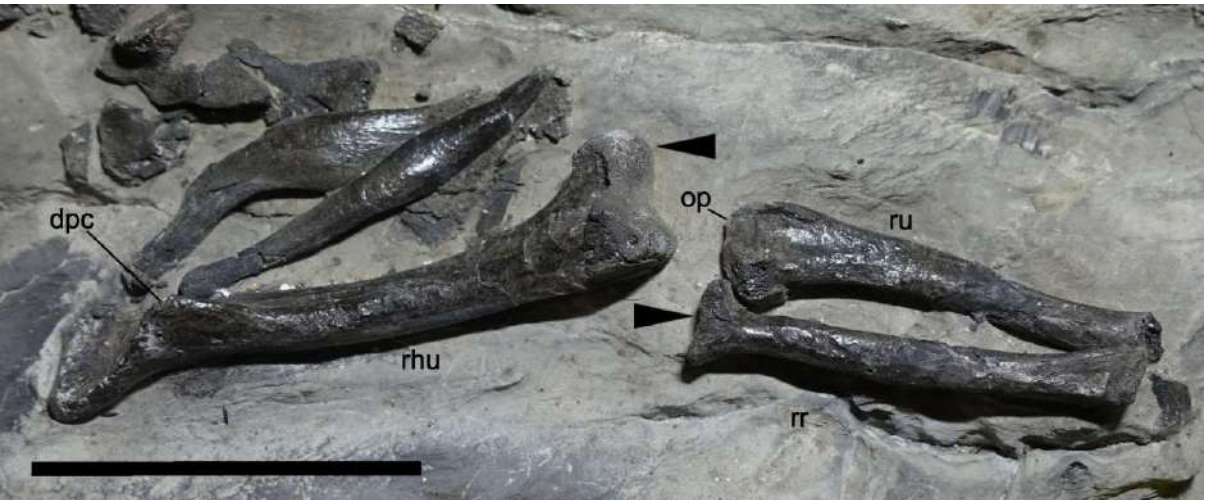
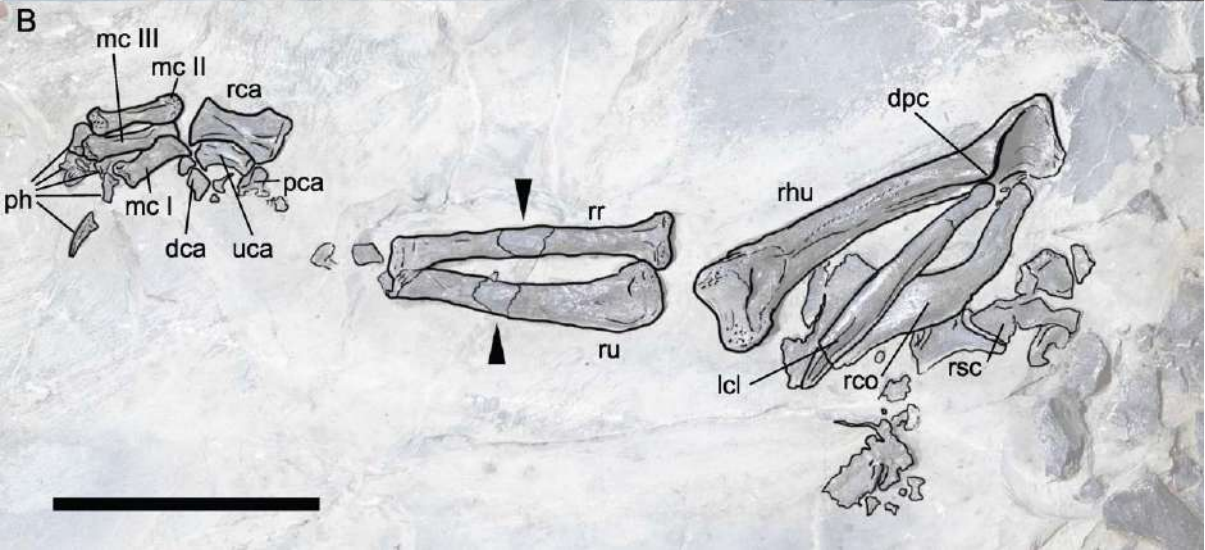


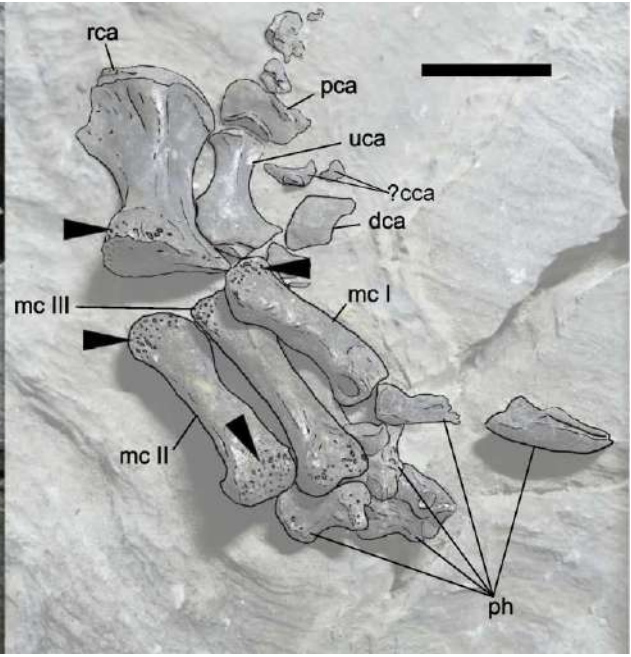
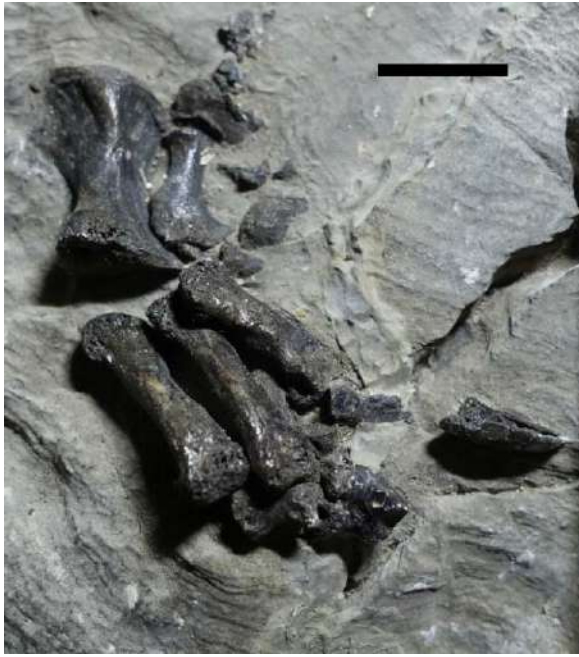
MCSNT 57248



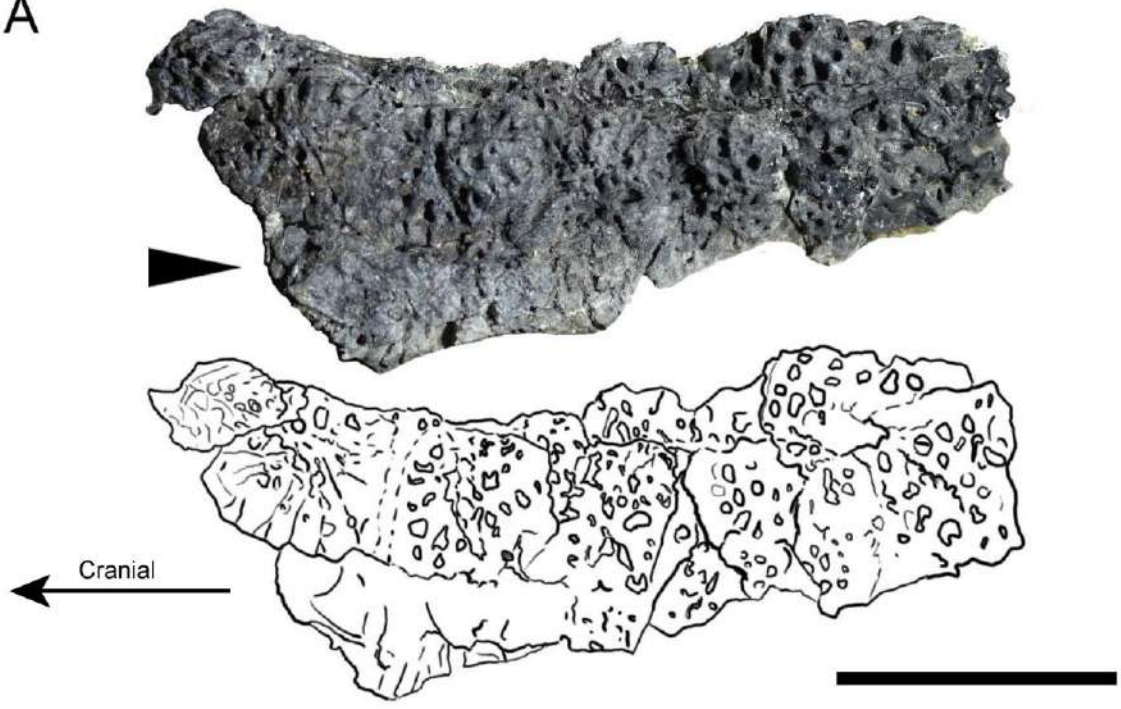




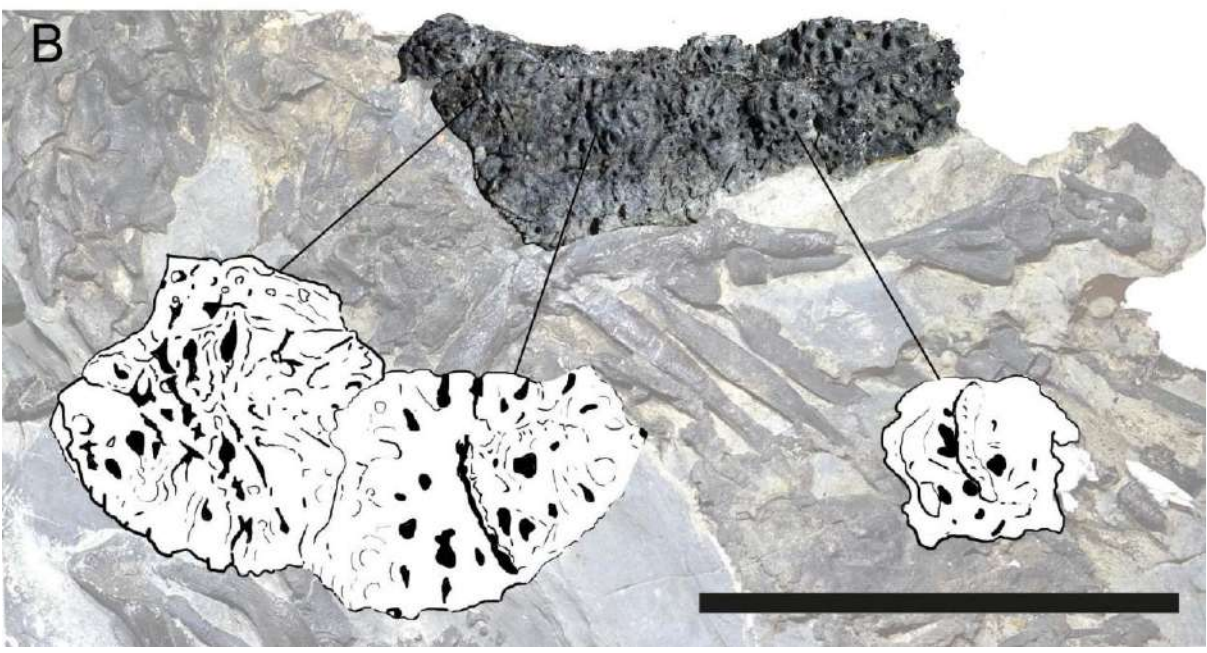




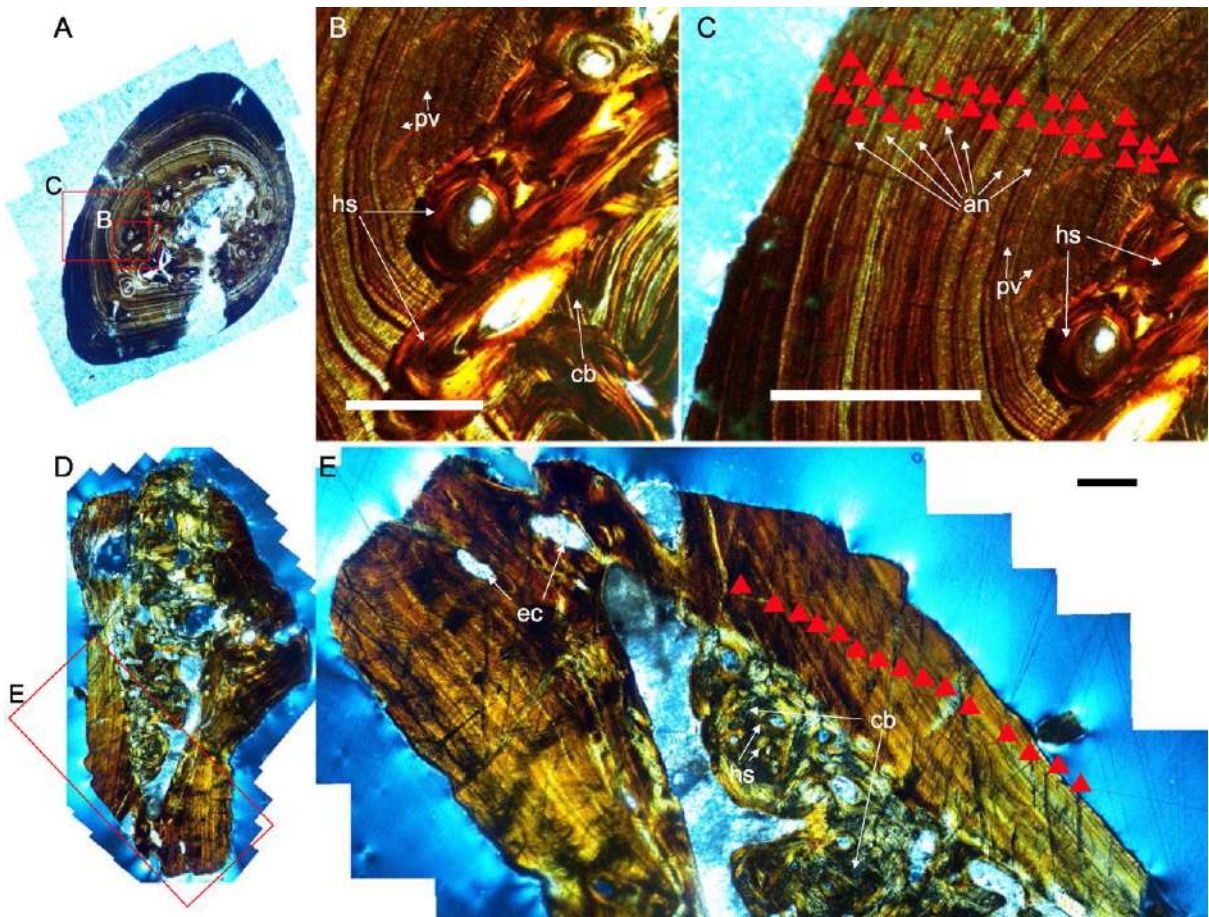
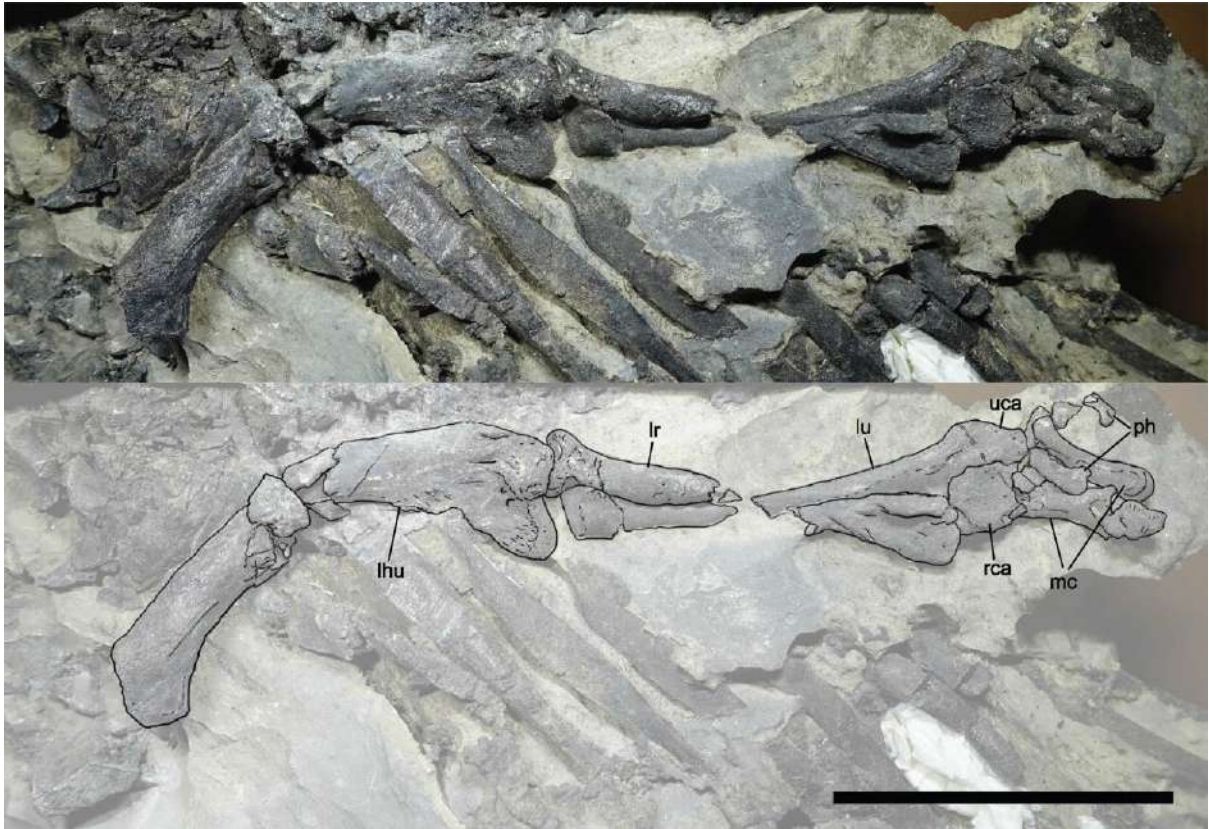
A

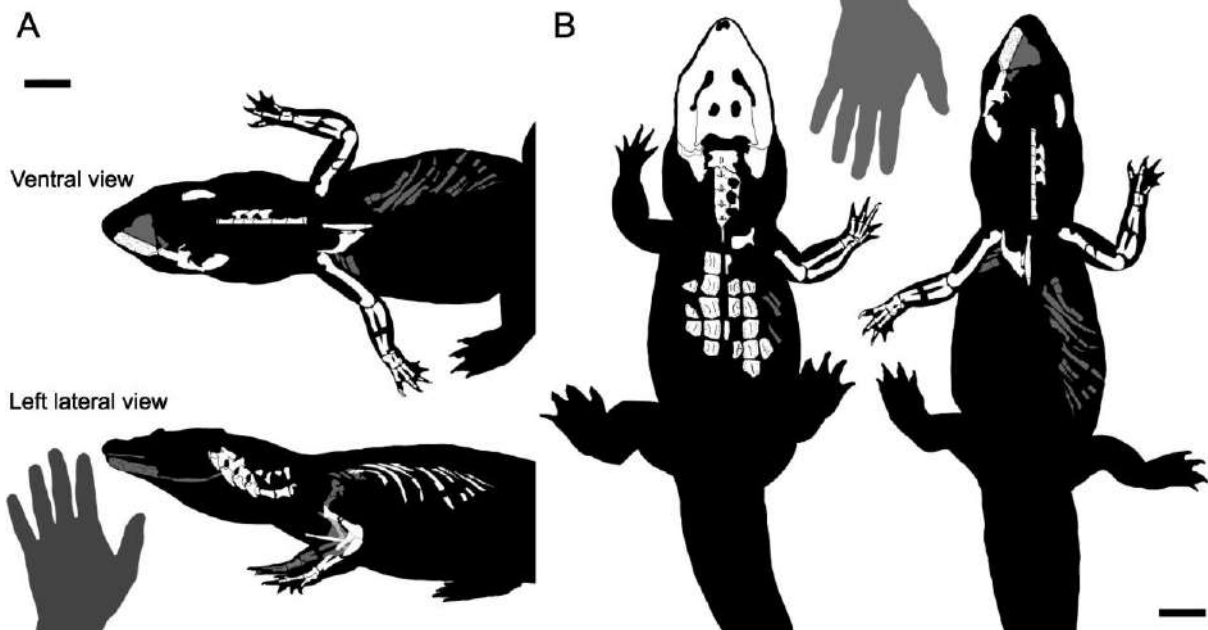
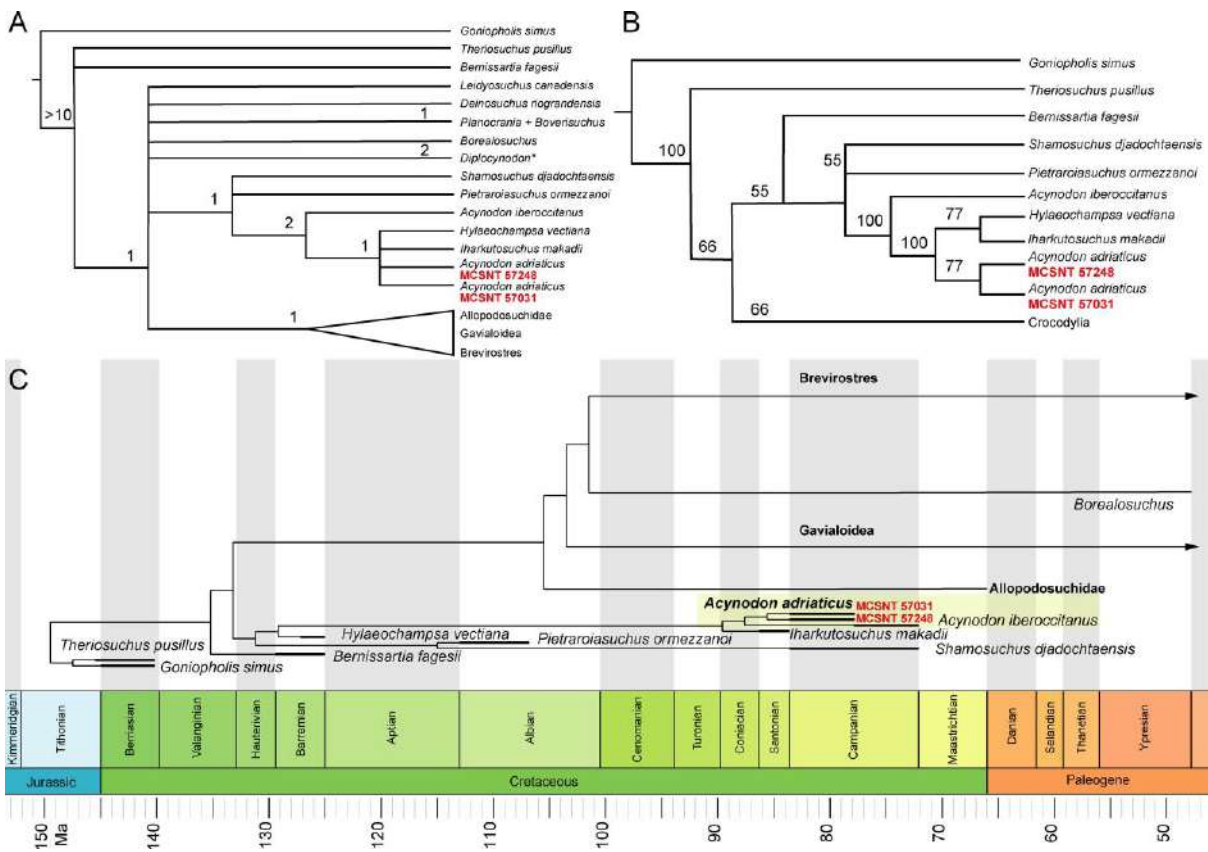


B









- New specimen of *Acynodon adriaticus* is herein osteologically and osteohistologically described in detail.
- Results from maximum parsimony phylogenetic analyses indicate a paraphyletic *Acynodon*.
- Results from bayesian phylogenetic analyses indicate a monophyletic *Acynodon*.
- The Middle–Late Campanian age of the Adriatic taxon support the Bayesian results.

**Declaration of interests**

The authors declare that they have no known competing financial interests or personal relationships that could have appeared to influence the work reported in this paper.

The authors declare the following financial interests/personal relationships which may be considered as potential competing interests: